Supporting Information

for

Multistep synthesis and X-ray structure of the carboxyl-terminated hybrid iron(II) phthalocyaninatoclathrochelates and their postsynthetic transformation into polytopic carboranyl-containing derivatives

Alexander S. Chuprin[a], Alexander A. Pavlov[a,b], Anna V. Vologzhanina[a], Pavel V. Dorovatovskii[c], Anton V. Makarenkov[a], Valentina A. Olshevskaya[a], Semyon V. Dudkin[a], and Yan Z. Voloshin[a,d]

[a]*Nesmeyanov Institute of Organoelement Compounds of the Russian Academy of Sciences, 28 bld 1. Vavilova st., 119334 Moscow, Russia*

[b]*BMSTU Center of National Technological Initiative "Digital Material Science: New Material and Substances", Bauman Moscow State Technical University, 2nd Baumanskaya st. 5, 105005, Moscow, Russia*

[c]*National Research Center Kurchatov Institute, 1 Kurchatova pl., 123098, Moscow, Russia*

[d]*Kurnakov Institute of General and Inorganic Chemistry of the Russian Academy of Sciences, 31 Leninsky pr., 119991 Moscow, Russia*

[@]*Corresponding author E-mail: voloshin@ineos.ac.ru*

Analytical and Spectral data

Fe(HNx)$_2$Nx(B4-C$_6$H$_4$COOH)

Anal. calcd. for $C_{25}H_{31}BFeN_6O_8$: C, 49.21; H, 5.12; N, 13.77. Found (%): C, 49.45; H, 5.03; N, 13.91. HR MS (MALDI-TOF): *m/z*: 611.0266 [M + H$^+$]$^+$. ^{1}H NMR (CD_2Cl_2, δ, ppm): 1.77 (s, 12H, *β*-CH_2), 2.88 (s, 12H, *α*-CH_2), 7.77 (d, 2H, 3-Ar), 8.02 (d, 2H, 2-Ar). ^{13}C{^{1}H} NMR (CD_2Cl_2, δ, ppm): 22.03 (s, *β'*-CH_2), 22.14 (s, *β*-CH_2), 26.94 (s, *α'*-CH_2), 27.00 (s, *α*-CH_2), 129.34 (s, 2-Ar), 132.33 (s, 3-Ar), 156.03 (s, HON=C, BON=C), 170.98 (s, COOH). Deconvoluted UV–vis (CH_2Cl_2): ν_{max}, cm^{-1} (ε · 10^{-3}, mol^{-1} L cm^{-1}): 42475 (23), 40264 (3.2), 34171 (7.8), 30173 (3.0), 25620 (1.1), 21039 (6.8), 19661 (1.0).

FeNx$_3$(B4-C$_6$H$_4$COOH)(ZrPc)

Anal. Calcd. for $C_{57}H_{45}N_{14}O_8FeBZr$: C, 56.49; H, 3.74; N, 16.18. Found (%): C, 56.66; H, 3.79; N, 16.03. HR MS (MALDI-TOF): *m/z*: 1211.2831 [M] $^{+\bullet}$. ^{1}H NMR (pyridine-*d$_5$*, δ, ppm): 0.72 (s, 12H, *β*-CH_2, *β'*-CH_2), 1.30 (m, 6H, *α'*-CH_2) 2.08 (t, 6H, *α*-CH_2), 5.09 (br. s, 1H, COOH), 7.94 (d, 2H, 3-Ar), 8.35 (m, 8H, *β*-Pc), 8.41 (d, 2H, 2-Ar), 9.77 (m, 8H, *α*-Pc). ^{13}C{^{1}H} NMR (pyridine-*d$_5$*, δ, ppm): 21.16 (s, *β'*-CH_2), 21.38 (s, *β*-CH_2), 25.39 (s, *α'*-CH_2), 26.01 (s, *α*-CH_2), 124.16 (s, *α*-Pc), 126.28 (s, 4-Ar), 129.15 (s, 3-Ar), 131.48 (s, β-Pc), 132.78 (s, 2-Ar), 138.26 (s, C(Pc)), 152.45 (s, C=N (Hf-capped)), 153.72 (s, C=N (B-capped)), 154.62 (s, C=N (Pc)), 169.94 (s, COOH). Deconvoluted UV–vis (C_5H_5N): ν_{max}, cm^{-1} (ε · 10^{-3}, mol^{-1} L cm^{-1}): 30501 (45), 29714 (24), 28408 (23), 27802 (19), 22328 (5.5), 20677 (12), 18131 (1.3), 17284 (5.5), 16809 (4.0), 16120 (13), 15973 (28), 15132 (32), 14893 (8.1), 14489 (224), 14322 (14).

FeNx$_3$(B4-C$_6$H$_4$COOH)(HfPc)

Anal. Calcd. for $C_{57}H_{45}N_{14}O_8FeBHf$: C, 52.70; H, 3.49; N, 15.09. Found (%): C, 52.47; H, 3.60; N, 14.92. HR MS (MALDI-TOF): *m/z*: 1299.3449 [M] $^{+\bullet}$. ^{1}H NMR (pyridine-*d$_5$*, δ, ppm): 0.74 (s, 12H, *β*-CH_2, *β'*-CH_2), 1.38 (t, 6H, *α'*-CH_2) 2.07 (t, 6H, *α*-CH_2), 5.05 (br. s, 1H, COOH + H_2O), 7.95 (d, 2H, 3-Ar), 8.37 (m,

8H, *β*-Pc), 8.41 (d, 2H, 2-Ar), 9.81 (m, 8H, *α*-Pc). $^{13}C\{^1H\}$ NMR (pyridine-d_5, δ, ppm): 21.18 (s, *β'*-CH_2), 21.45 (s, *β*-CH_2), 25.41 (s, *α'*-CH_2), 26.02 (s, *α*-CH_2), 124.16 (s, *α*-Pc), 129.15 (s, 3-Ar), 131.57 (s, β-Pc), 132.80 (s, 2-Ar), 138.34 (s, C(Pc)), 152.99 (s, C=N (Hf-capped)), 153.60 (s, C=N (B-capped)), 154.92 (s, C=N (Pc)). Deconvoluted UV–vis (C_5H_5N): ν_{max}, cm^{-1} ($\varepsilon \cdot 10^{-3}$, mol^{-1} L cm^{-1}): 30180 (50), 29544 (25), 28338 (26), 27100 (8.3), 22909 (5.9), 20846 (16), 17788 (3.2), 17293 (4.1), 16824 (3.7), 16123 (13), 15961 (27), 15137 (30), 14904 (9.9), 14494 (215), 14343 (12).

Fe(HNx)$_2$Nx(B4-C_6H_4COProp)

Anal. Calcd. for $C_{28}H_{34}N_7O_7FeB$: C, 51.96; H, 5.29; N, 15.15. Found (%): C, 52.06; H, 5.23; N, 15.00. HR MS (MALDI-TOF): *m/z*: 648.1949 $[M + H^+]^+$. ^1H NMR (CD_2Cl_2, δ, ppm): 1.75 (s, 12H, *β*-CH_2), 2.33 (t, 1H, $NHCH_2CC\underline{H}$), 2.88 (s, 12H, *α*-CH_2), 4.23 (m, dd, 2H, $NHC\underline{H}_2CCH$), 6.38 (t, 1H, $N\underline{H}CH_2CCH$), 7.71 (dd, 4H, Ph). $^{13}C\{^1H\}$ NMR (CD_2Cl_2, δ, ppm): 22.04 (s, *β'*-CH_2), 22.14 (s, *β*-CH_2), 26.95 (s, *α'*-CH_2) 27.01 (s, *α*-CH_2), 30.01 (s, $NH\underline{C}H_2CCH$), 71.61 (s, $NHCH_2C\underline{C}H$), 80.57 (s, $NHCH_2\underline{C}CH$), 126.24 (s, Ph), 132.42 (s, Ph), 155.95, 156.04 (two s, HON=C, BON=C), 167.74 (s, C=O). Deconvoluted UV–vis (CH_2Cl_2): ν_{max}, cm^{-1} ($\varepsilon \cdot 10^{-3}$, mol^{-1} L cm^{-1}): 42949 (26), 39866 (3.8), 34311 (7.8), 30199 (2.2), 25365 (1.3), 21259 (8.6), 19628 (1.9).

FeNx$_3$(B4-C_6H_4COProp)(ZrPc)

Anal. Calcd. for $C_{60}H_{48}N_{15}O_7FeBZr$: C, 57.70; H, 3.87; N, 16.82. Found (%): C, 57.86; H, 3.83; N, 16.99. MS (MALDI-TOF): *m/z*: 1248.4294 $[\ M\ ]^{+\bullet}$. ^1H NMR (pyridine-d_5, δ, ppm): 0.66 (s, 12H, *β*-CH_2, *β'*-CH_2), 1.22 (m, 6H, *α'*-CH_2), 2.00 (t, 6H, *α*-CH_2), 2.99 (s, 1H, $NHCH_2CC\underline{H}$), 4.41 (s, 2H, $NHC\underline{H}_2CCH$), 7.86 (d, 2H, 3-Ar), 8.22 (d, 2H, 2-Ar), 8.31 (m, 8H, *β*-Pc), 9.64 – 9.69 (m, 9H, NH, *α*-Pc). $^{13}C\{^1H\}$ NMR (pyridine-d_5, δ, ppm): 21.12 (s, *β'*-CH_2), 21.33 (s, *β*-CH_2), 25.32 (s, *α'*-CH_2), 25.94 (s, *α*-CH_2), 29.70 (s, $NH\underline{C}H_2CCH$), 72.25 (s, $NHCH_2C\underline{C}H$), 82.31 (s, $NHCH_2\underline{C}CH$), 124.16 (s, α-Pc), 126.93 (s, 3-Ar), 130.41 (s, C_{ipso}(Ar)), 131.39

(s, β-Pc), 132.74 (s, 2-Ar), 138.18 (s, C(Pc)), 152.35 (s, C=N (Zr-capped)), 153.60 (s, C=N (B-capped)), 154.46 (s, C=N (Pc)), 168.30 (s, C=O). Deconvoluted UV–vis (C_5H_5N): ν_{max}, cm^{-1} ($\varepsilon \cdot 10^{-3}$, mol^{-1} L cm^{-1}): 30598 (43), 29676 (26), 28384 (28), 27454 (13), 22289 (6.5), 20609 (12), 18057 (1.6), 17282 (5.1), 16814 (3.9), 16119 (12), 15969 (27), 15135 (31), 14895 (8.4), 14490 (217), 14307 (13).

Fe(HNx)$_2$Nx(B4-C$_6$H$_4$COSpCarb)

Anal. Calcd. for $C_{31}H_{47}N_{10}O_7FeB_{11}$: C, 43.98; H, 5.60; N, 16.55. Found (%): C, 43.81 H, 5.38; N, 16.77. HR MS (MALDI-TOF): *m/z*: 847.5160 $[M + H^+]^+$, 869.4871 $[M + Na^+]^+$, 885.4914 $[M + K^+]^+$. ^{1}H NMR (CD_2Cl_2, δ, ppm): 1.75 (s, 12H, *β*-CH_2), 2.02 (br. s, 2H, B–H (Carb)), 2.28 (br. s, 6H, B–H (Carb)), 2.48 (br. s, 1H, B9), 2.55 (br. s, 1H, B12), 2.87 (s, 12H, *α*-CH_2), 3.93 (s, 1H, C–H (Carb)), 4.70 (d, 2H, $NHCH_2$), 5.02 (s, 2H, NCH_2), 6.86 (t, 1H, NH), 7.72 (m, 5H, Ph, 5H-triazole). ^{11}B{^{1}H} NMR (CD_2Cl_2, δ, ppm): –12.58 (s, 4B, B3, B6, B7, B11), –11.64 (s, 2B, B4, B5), –9.42 (s, 2B, B8, B10), –4.56 (s, 1B, B9), –1.49 (s, 1B, B12), 6.80 (m, 1B, B–Ar). ^{13}C{^{1}H} NMR (CD_2Cl_2, δ, ppm): 22.05 (s, *β'*-CH_2), 22.15 (s, *β*-CH_2), 26.93 (s, *α'*-CH_2) 27.00 (s, *α*-CH_2), 35.83 (s, NH$\underline{C}H_2$), 59.77 (s, N$\underline{C}H_2$), 124.47 (s, 5H-triazole), 126.23 (s, Ph), 132.43 (s, Ph), 155.93, 156.00 (two s, HON=C, BON=C). Deconvoluted UV–vis (CH_2Cl_2): ν_{max}, cm^{-1} ($\varepsilon \cdot 10^{-3}$, mol^{-1} L cm^{-1}): 43343 (33), 39462 (5.5), 35403 (5.5), 32533 (4.6), 25625 (1.8), 21399 (11), 19773 (1.3).

FeNx$_3$(B4-C$_6$H$_4$COSpCarb)(ZrPc)

Anal. Calcd. for $C_{63}H_{61}N_{18}O_7FeB_{11}Zr$: C, 52.25; H, 4.25; N, 17.41. Found (%): C, 52.41, H, 4.28; N, 17.27. HR MS (MALDI-TOF): *m/z*: 1446.8815 $[M]^{+\bullet}$. ^{1}H NMR ($CDCl_3$, δ, ppm): 1.13 (m, 12H, *β'*-, *β*-CH_2), 1.21 (t, 6H, *α'*-CH_2), 2.03 (br. s, 2H, B–H (Carb)), 2.13 (t, 6H, *α*-CH_2), 2.28 (br. s, 6H, B–H (Carb)), 2.37 (br. s, 1H, B9), 2.48 (br. s, 1H, B12), 3.75 (s, 1H, C–H (Carb)), 4.58 (d, 2H, $NHCH_2$), 4.88 (s, 2H, NCH_2), 6.60 (t, 1H, NH), 7.32 (d, 2H, Ph), 7.43 (d, 2H, Ph), 7.60 (m, 1H, 5H-triazole), 8.22 (m, 8H, *β*-Pc), 9.50 (m, 8H, *α*-Pc), ^{11}B{^{1}H} NMR ($CDCl_3$,

δ, ppm): –12.89 (s, 4B, B3, B6, B7, B11), –11.86 (s, 2B, B4, B5), –9.61 (s, 2B, B8, B10), –4.45 (s, 1B, B9), –1.27 (s, 1B, B12), 6.97 (m, 1B, B–Ar). $^{13}C\{^{1}H\}$ NMR (pyridine-d_5, δ, ppm): 21.01 (s, *β'*-CH_2), 21.21 (s, *β*-CH_2), 25.18 (s, *α'*-CH_2), 25.84 (s, *α*-CH_2), 36.28 (s, N$\underline{C}H_2$), 59.01 (s, $NHCH_2$), 124.16 (s, α-Pc), 124.41 (s, 5H-triazole), 126.86 (s, Ph), 131.25 (s, β-Pc), 132.64 (s, Ph), 138.00 (s, C(Pc)), 152.19 (s, C=N (*α*-CH_2)), 153.48 (s, C=N (*α'*-CH_2)), 154.18 (s, C=N (Pc)), 168.58 (s, C=O). Deconvoluted UV–vis (C_5H_5N): ν_{max}, cm^{-1} ($\varepsilon \cdot 10^{-3}$, mol^{-1} L cm^{-1}): 30690 (47), 29682 (24), 28373 (30), 27326 (11), 21886 (8.0), 20419 (9.4), 17638 (3.4), 17255 (4.0), 16812 (3.1), 16115 (12), 15943 (27), 15150 (27), 14908 (8.7), 14485 (200), 14354 (17).

UV-vis spectra

Initial carborane is known to be UV-silent in the spectral range under study (25000 – 43500 cm^{-1}). The spectrum of 1-[(*o*-carboran-1'-yl)methyl]-4-pentyl-1,2,3-triazole, used as a model carboranyl-based compound, contains in this range a very low-intensive band with maximum at 37879 cm^{-1} (see Table S2); a more intensive band in its UV-vis spectrum appeared at 45450 cm^{-1}. A performed functionalization of the propargylamine semiclathrochelate $FeNx(HNx)_2(B4\text{-}C_6H_4COProp)$ using its "click" reaction led to a slight (approximately 1100 cm^{-1}) shortwave shift of the corresponding absorption in the spectrum of thus obtained polytopic carboranyl-terminated iron(II) semiclathrochelate $FeNx(HNx)_2(B4\text{-}C_6H_4COSpCarb)$.

Spin state of the encapsulated iron(II) ion

The low-spin state of all the (pseudo)macrobicyclic iron(II) tris-α-dioximates is due to the following experimental data:

1. from ^{57} Mössbauer spectra for more than hundred complexes of this type (see, for example, [S1 – S4])

2. from the solution NMR data (the absence of any paramagnetic shift or paramagnetic broadening).

3. from the small values of Fe–N distances (approximately 1.90–1.94Å), in their X-rayed molecules, as compared with the high-spin iron(II) complexes with nitrogen donor ligands (typically 2.1–2.2Å). Indeed, the performed analysis of CBSD data for 427 known XRD structures of iron(II) tris(2,2-bipyridinates) and tris(4,10-phenanthrolinates) showed that the averaged Fe–N distance for them is equal to 1.98(2)Å. This value is characteristic of the LS $Fe^{II}N_6$-complexes, while those for the analogous HS iron(II) complexes typically exceed 2.1 Å (see, for example, a comparison of the LS and HS iron(II) complexes performed by Lecomte C. and co-authors [S5, S6].

The experimentally observed increase in (as compared with non-macrocyclic iron(II) tris-α-dioximates) and a very high ligand field strength, characteristic of a given type of iron(II) cage complexes [S1, S2], can be due to the so-called “macrobicyclic effect”. It is caused by formation of their quasiaromatic macrobicyclic and pseudomacrobicyclic polyazomethine ligands.

As a result, all the obtained (pseudo)macrobicyclic iron(II) tris-α-dioximates and their hybrid derivatives are the low-spin d^6 complexes in their ground state.

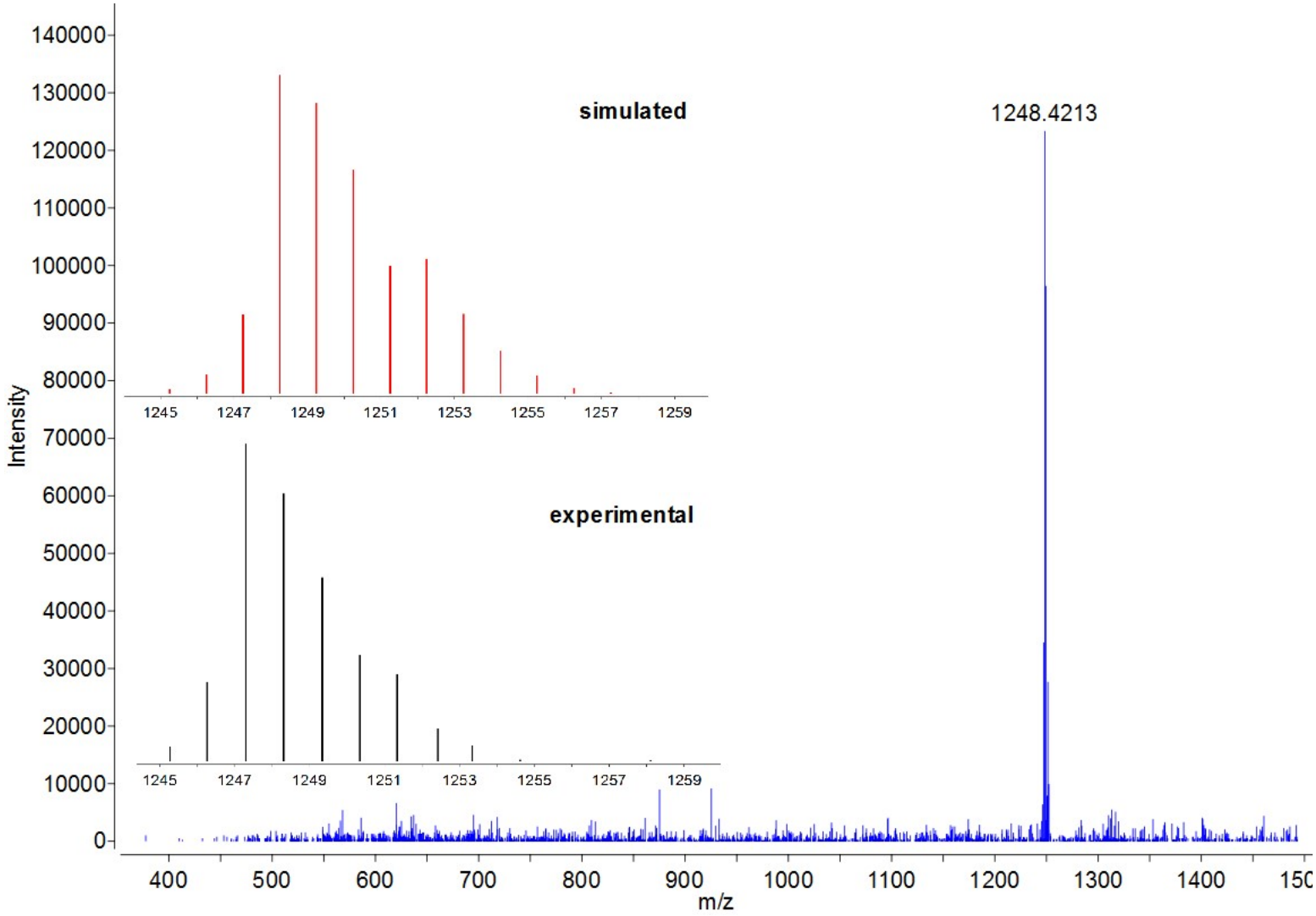

Figure S1. HR MALDI-TOF mass spectrum of the hybrid complex $FeNx_3$(B4-C_6H_4COProp)(ZrPc). Inset: the experimental and theoretically calculated isotopic distribution in the peaks of its molecular ion.

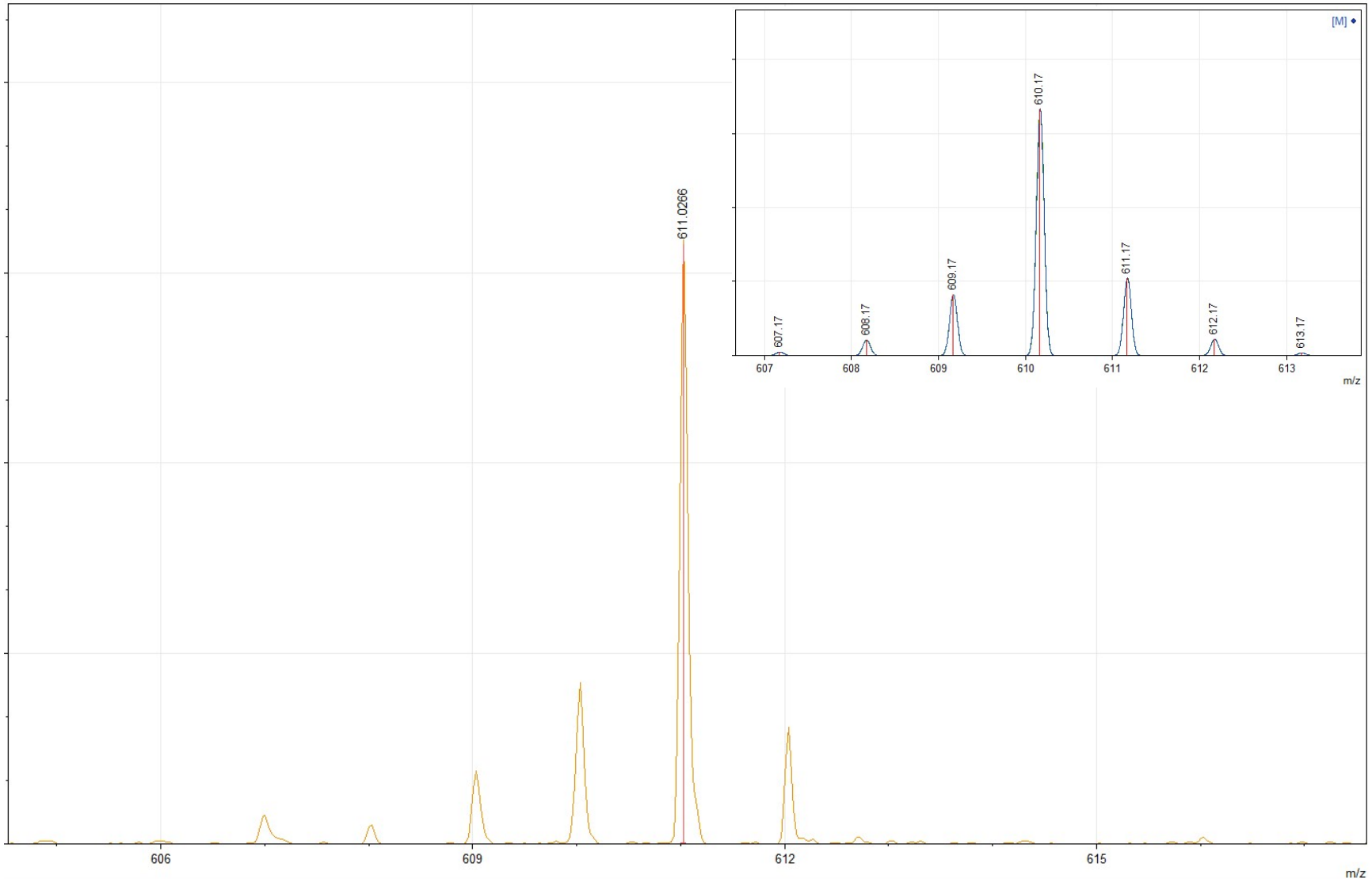

Figure S2. Fragment of the MALDI-TOF mass spectrum of the semiclathrochelate $FeNx(HNx)_2(B4\text{-}C_6H_4COOH)$ in its positive range. Insert: the theoretically calculated isotopic distribution in its molecular ion.

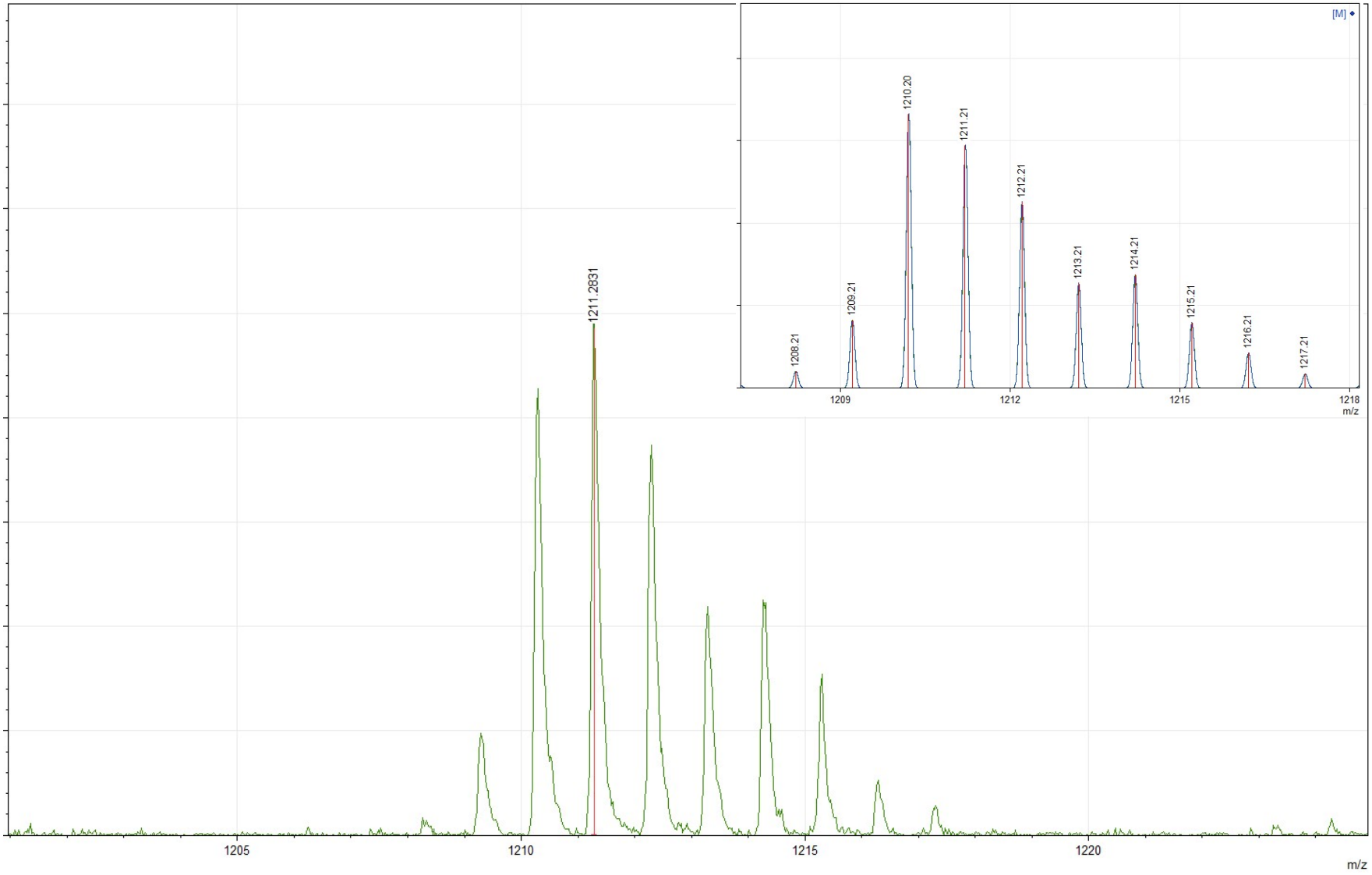

Figure S3. Fragment of the MALDI-TOF mass spectrum of the hybrid complex $FeNx_3(B4\text{-}C_6H_4COOH)(ZrPc)$ in its positive range. Insert: the theoretically calculated isotopic distribution in its molecular ion.

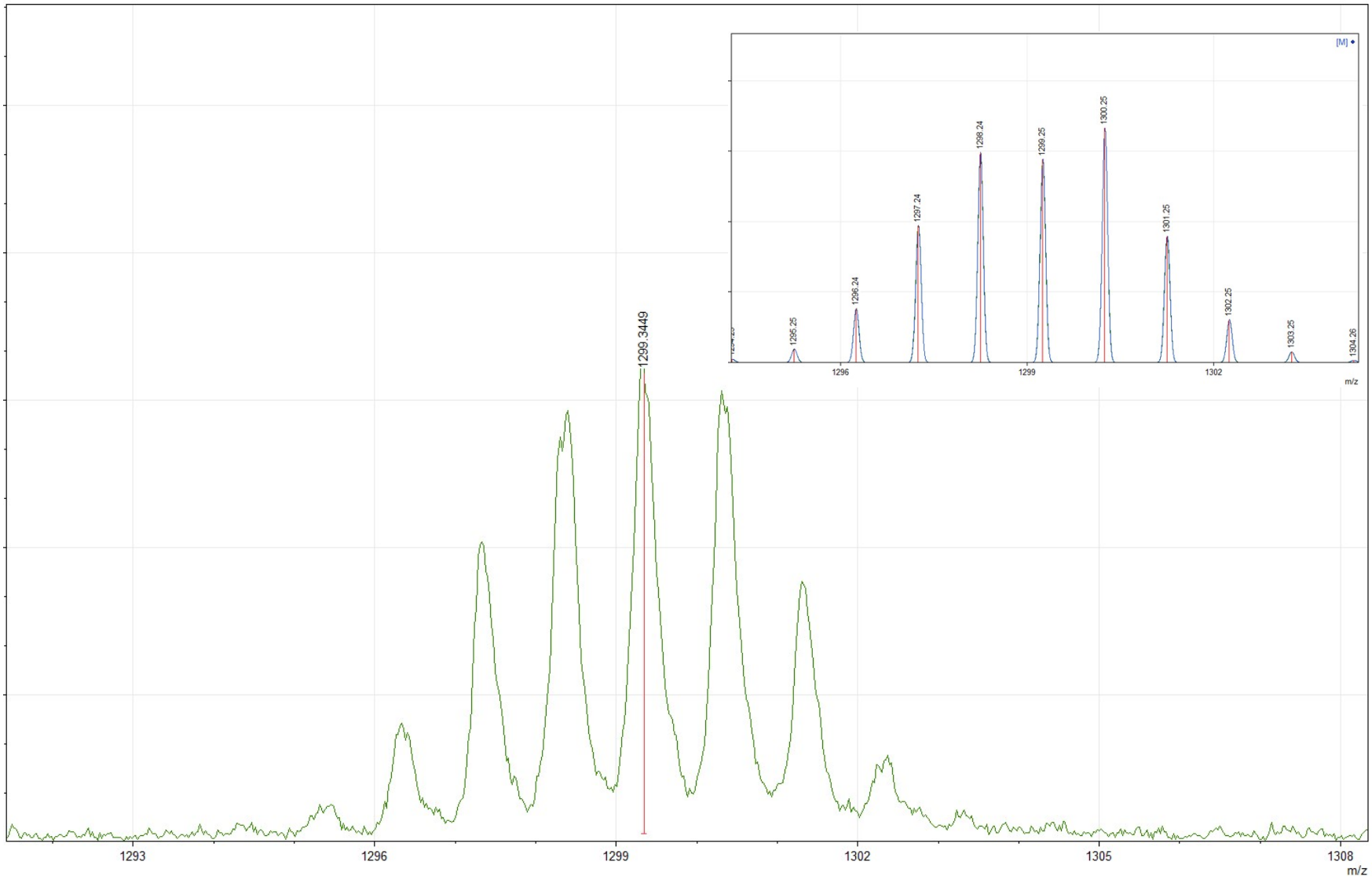

Figure S4. Fragment of the MALDI-TOF mass spectrum of the hybrid complex $FeNx_3$(B4-C_6H_4COOH)(HfPc) in its positive range. Insert: the theoretically calculated isotopic distribution in its molecular ion.

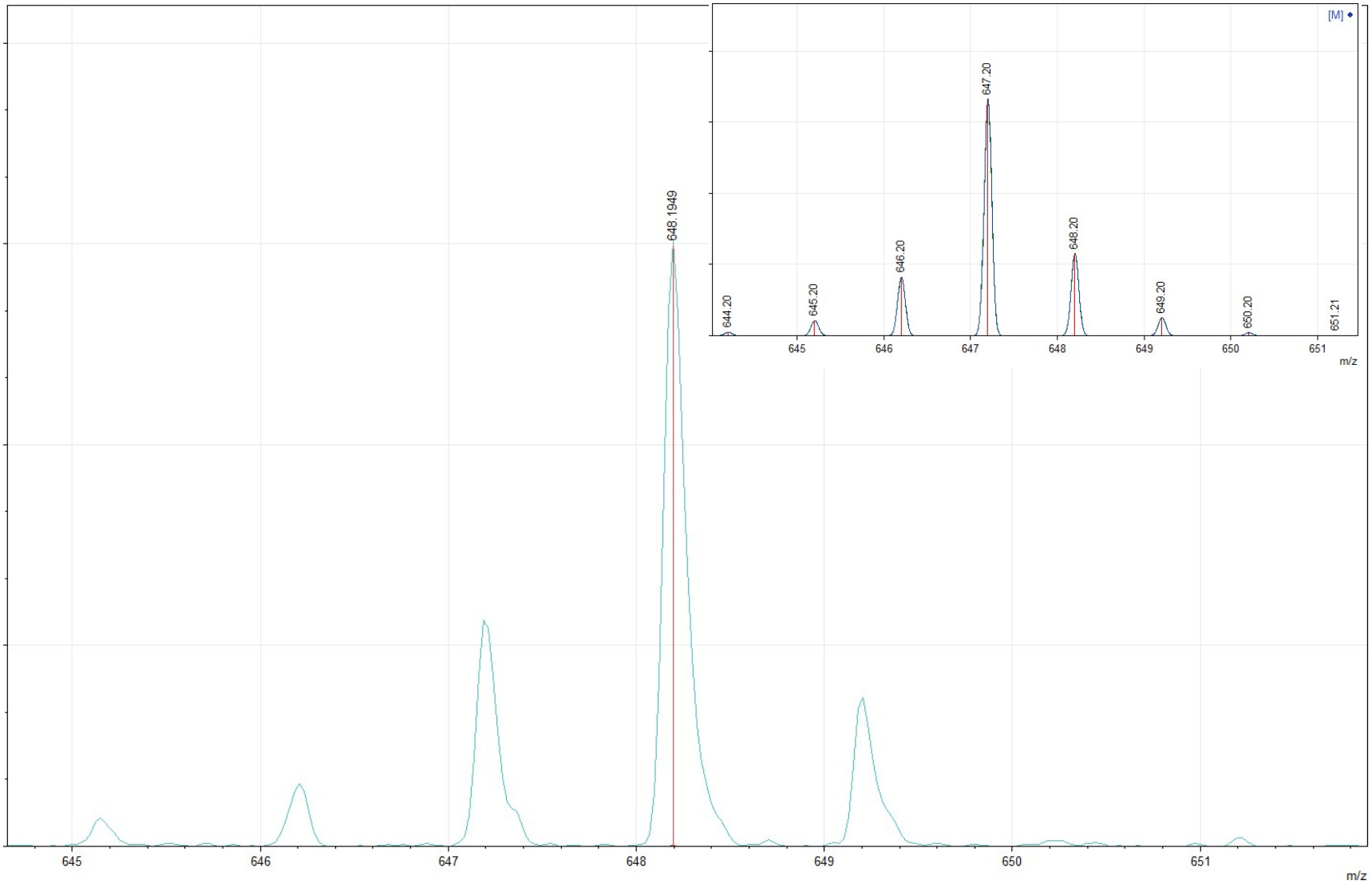

Figure S5. Fragment of the MALDI-TOF mass spectrum of the semiclathrochelate $FeNx(HNx)_2(B4\text{-}C_6H_4COProp)$ in its positive range. Insert: the theoretically calculated isotopic distribution in its molecular ion.

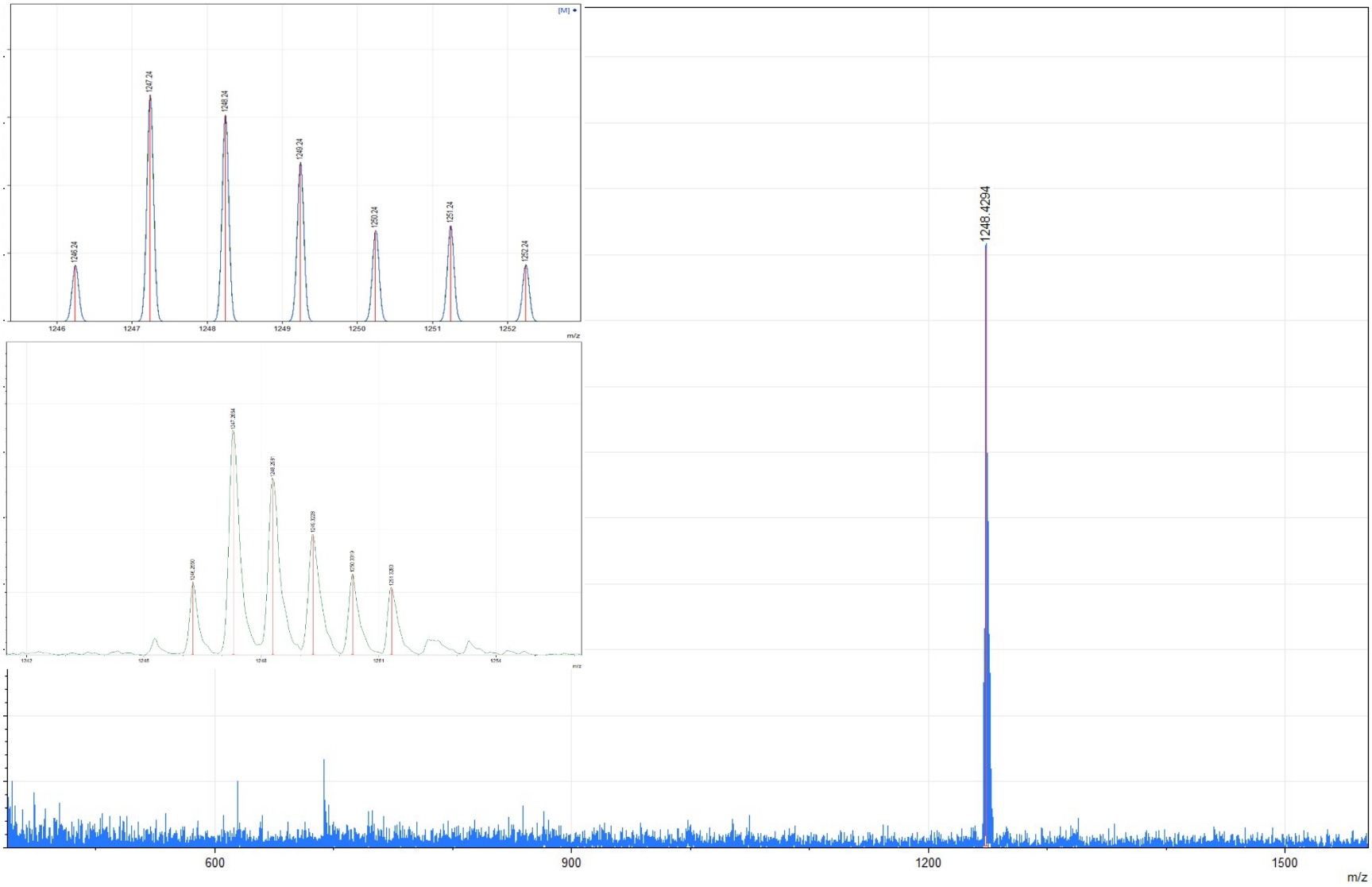

Figure S6. Fragment of the MALDI-TOF mass spectrum of the hybrid complex $FeNx_3$(B4-C_6H_4COProp)(ZrPc) in its positive range. Insert: the theoretically calculated isotopic distribution in its molecular ion.

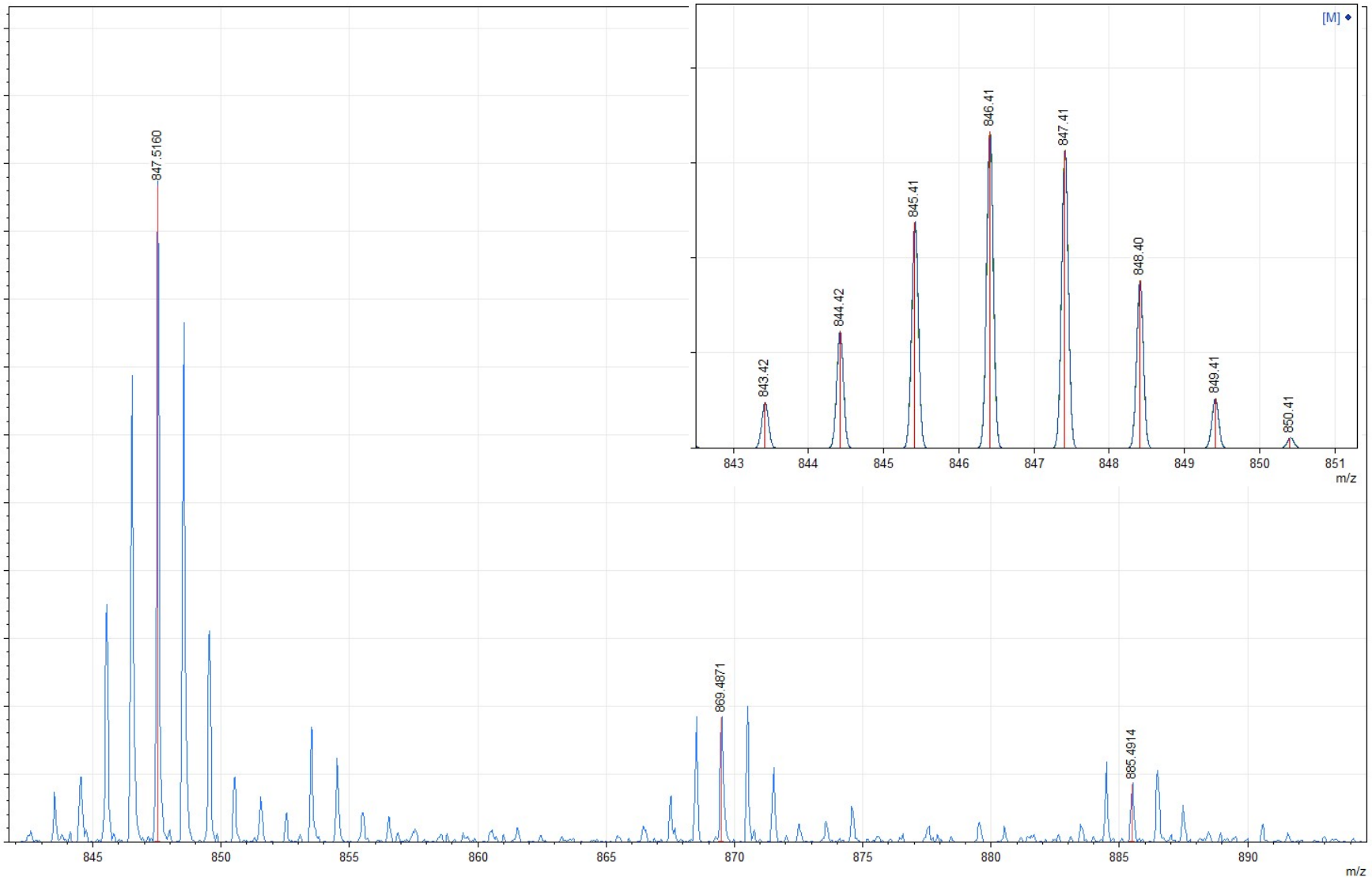

Figure S7. Fragment of the MALDI-TOF mass spectrum of the carboranosemiclathrochelate $FeNx(HNx)_2(B4\text{-}C_6H_4COSpCarb)$ in its positive range. Insert: the theoretically calculated isotopic distribution in its molecular ion.

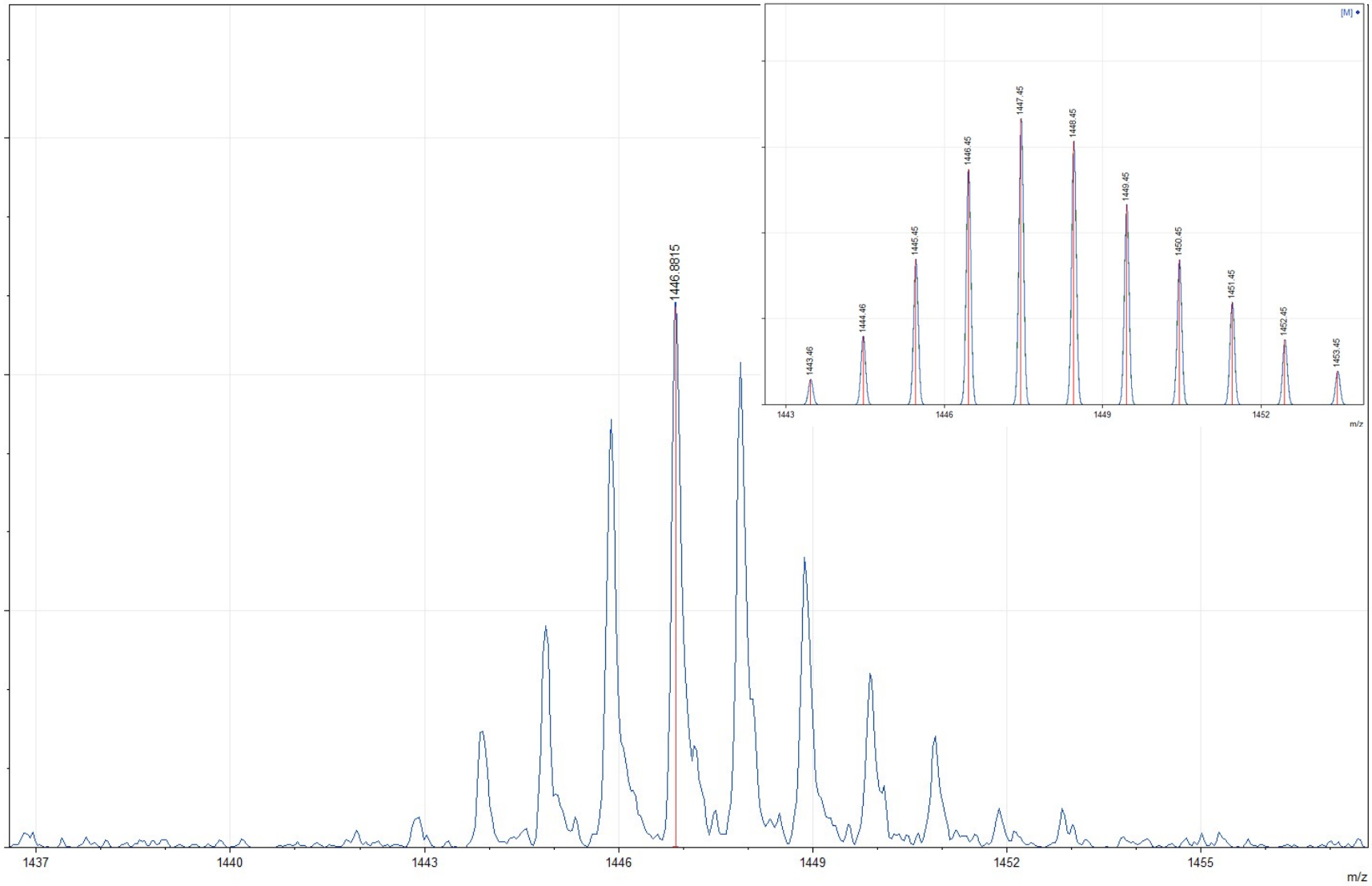

Figure S8. Fragment of the MALDI-TOF mass spectrum of the polytopic complex $FeNx_3$(B4-C_6H_4COSpCarb)(ZrPc) in its positive range. Insert: the theoretically calculated isotopic distribution in its molecular ion.

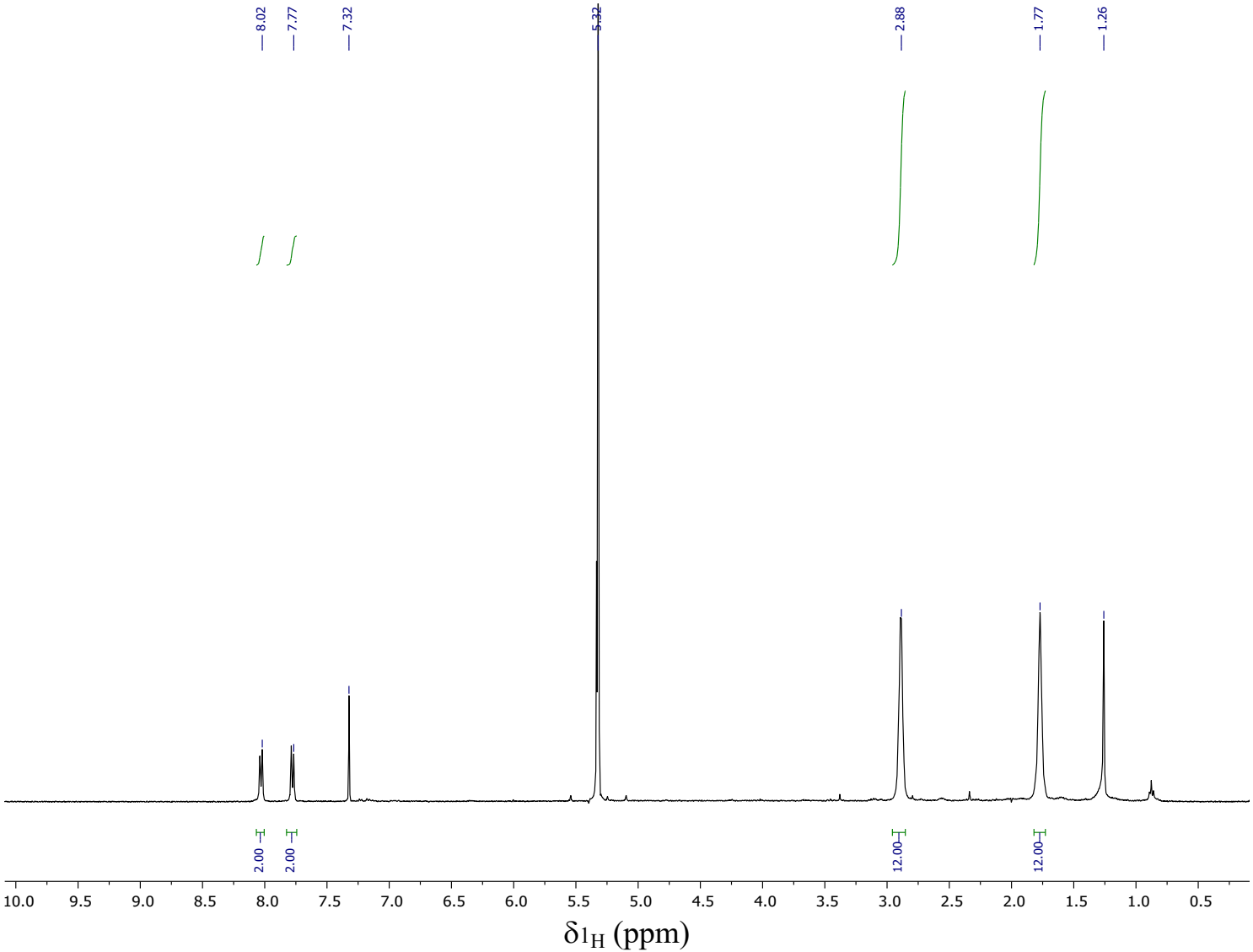

Figure S9. Solution ^{1}H NMR spectrum of the semiclatrochelate $Fe(HNx)_2Nx(B4\text{-}C_6H_4COOH)$ in CD_2Cl_2.

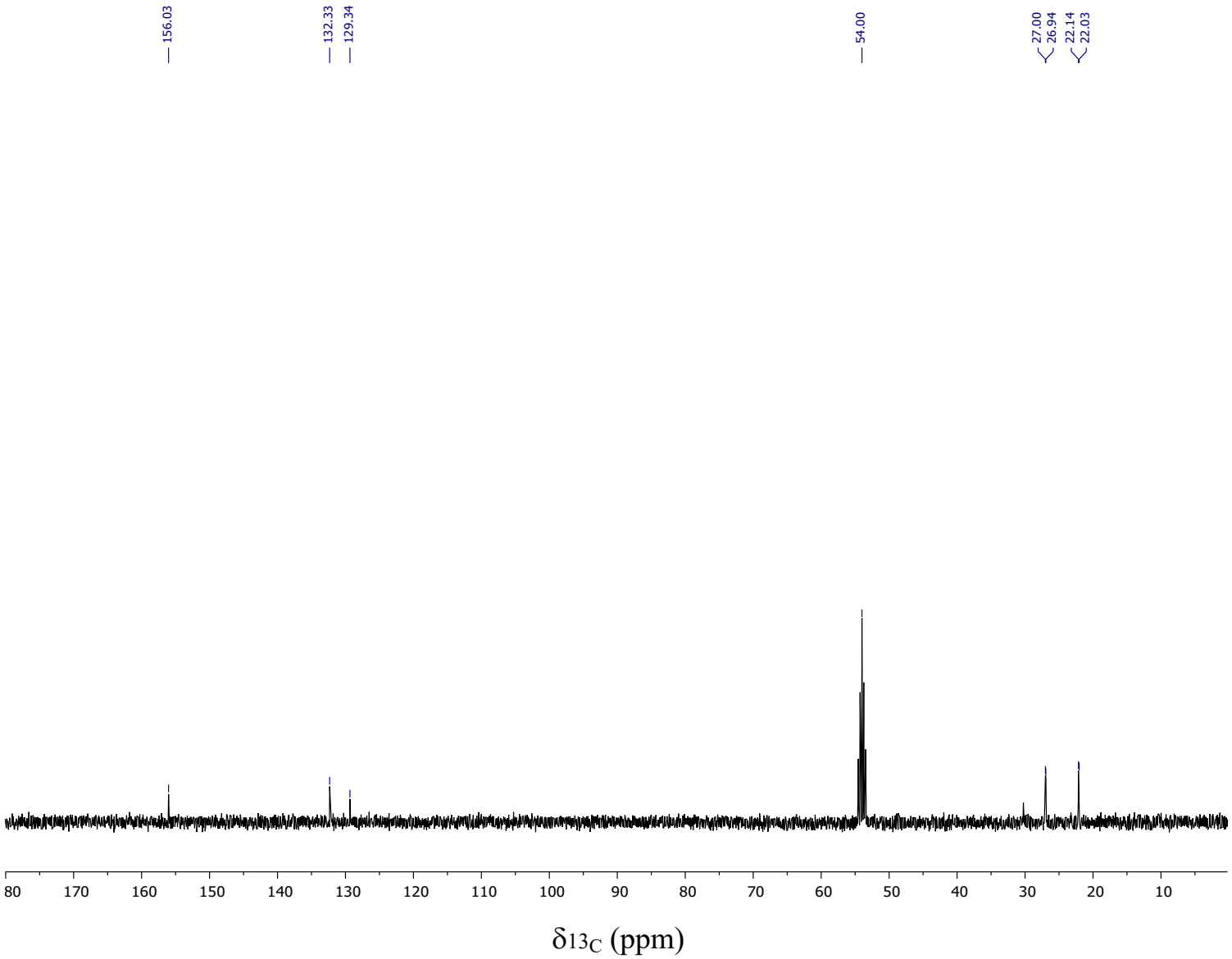

Figure S10. $^{13}C\{^{1}H\}$ NMR spectrum of the semiclatrochelate $Fe(HNx)_2Nx(B4\text{-}C_6H_4COOH)$ in CD_2Cl_2.

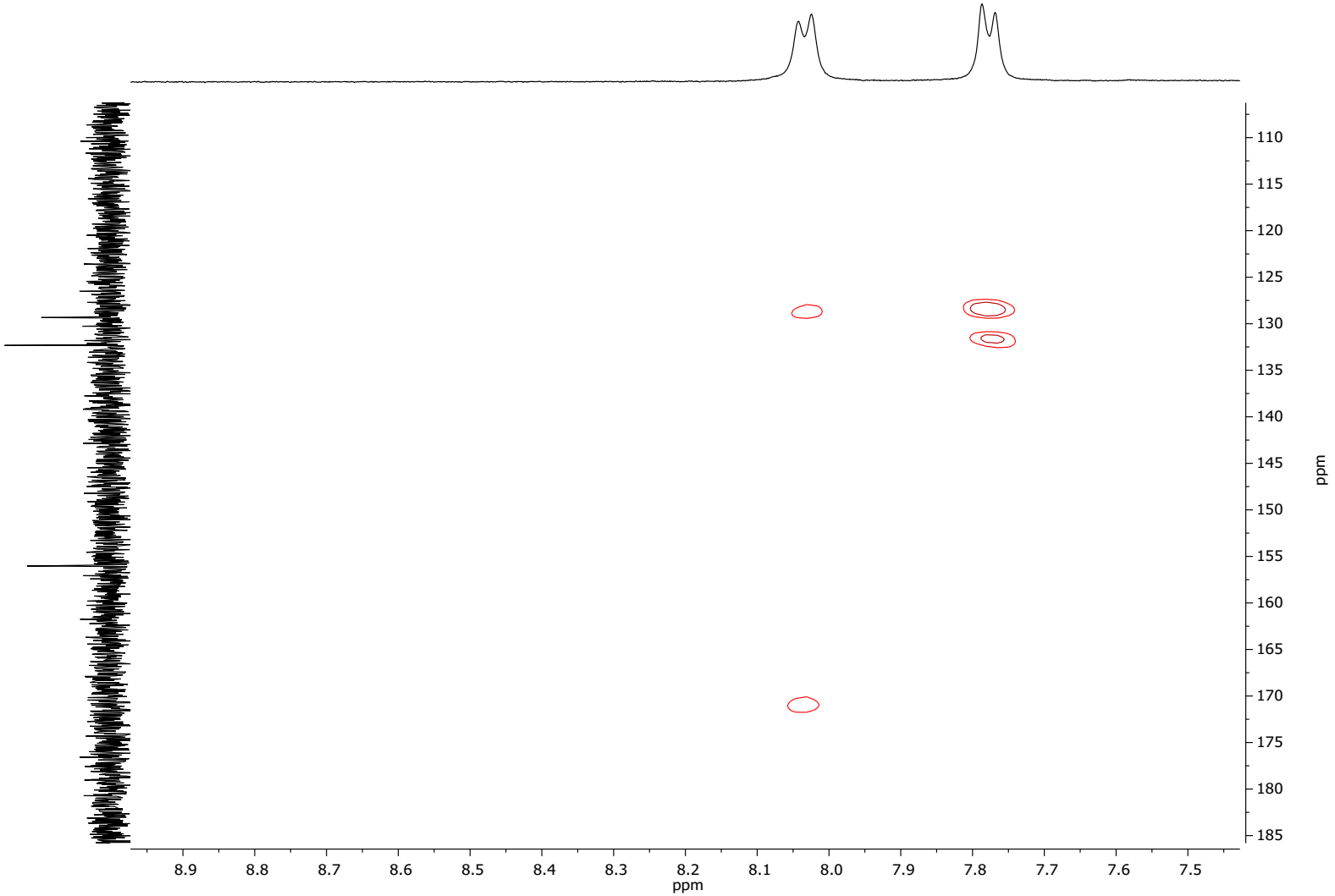

Figure S11. Fragment of 2D HMBC NMR spectrum of the semiclathrochelate $Fe(HNx)_2Nx(B4\text{-}C_6H_4COOH)$ in CD_2Cl_2.

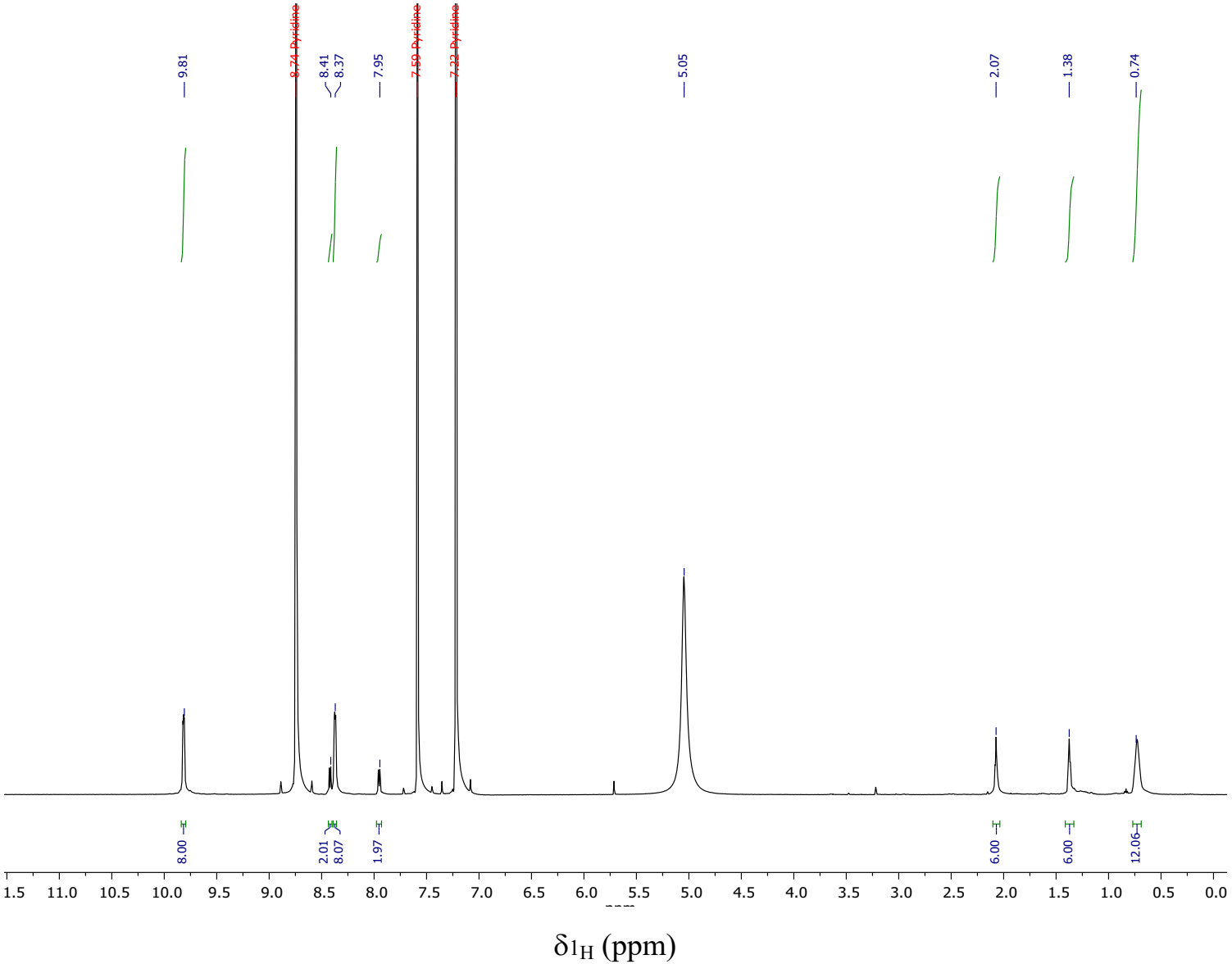

Figure S12. Solution ^{1}H NMR spectrum of the hybrid complex $FeNx_3$(B4-C_6H_4COOH)(HfPc) in pyridine-d_5.

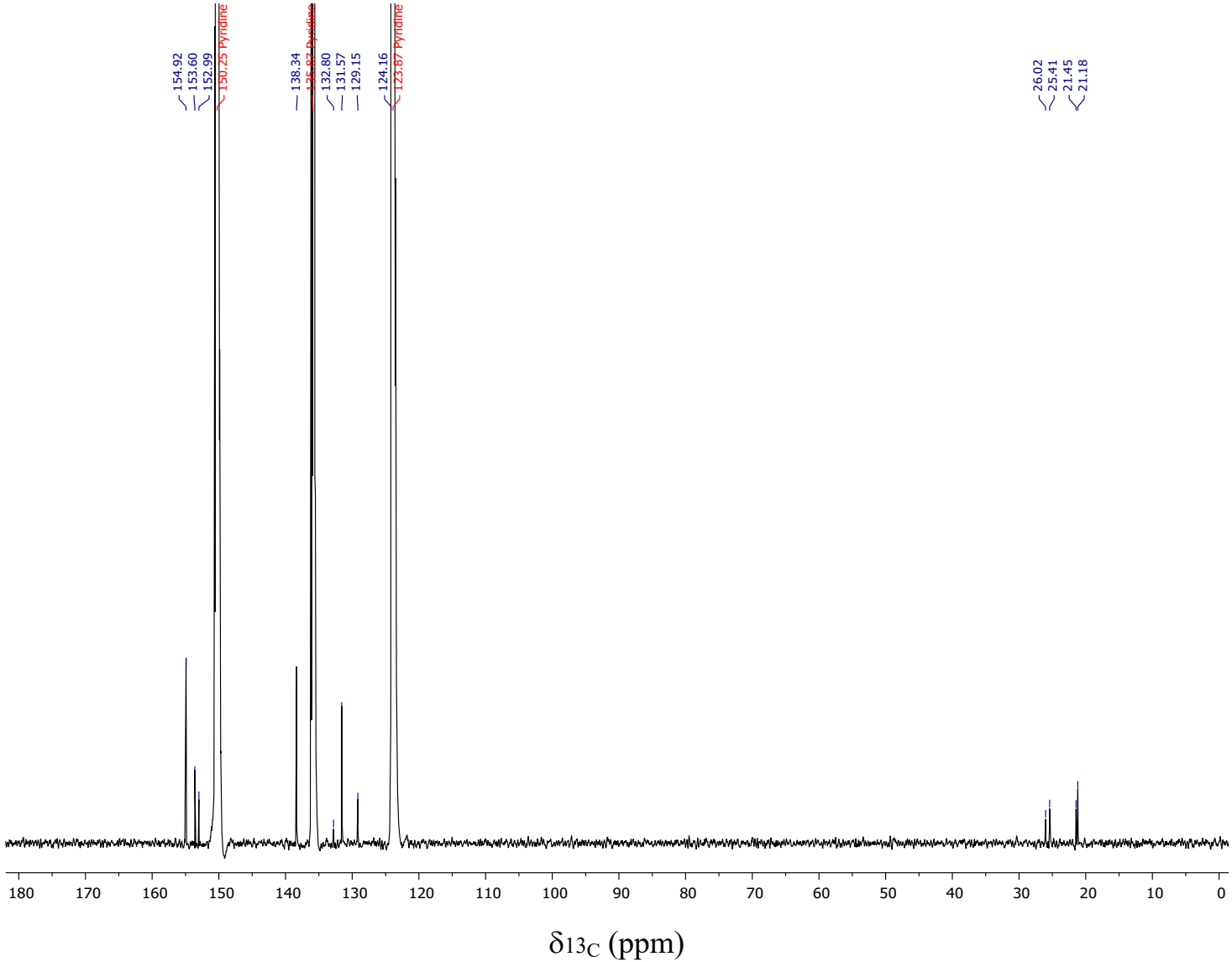

Figure S13. Solution $^{13}C\{^{1}H\}$ NMR spectrum of the hybrid complex $FeNx_3(B4\text{-}C_6H_4COOH)(HfPc)$ in pyridine-d_5.

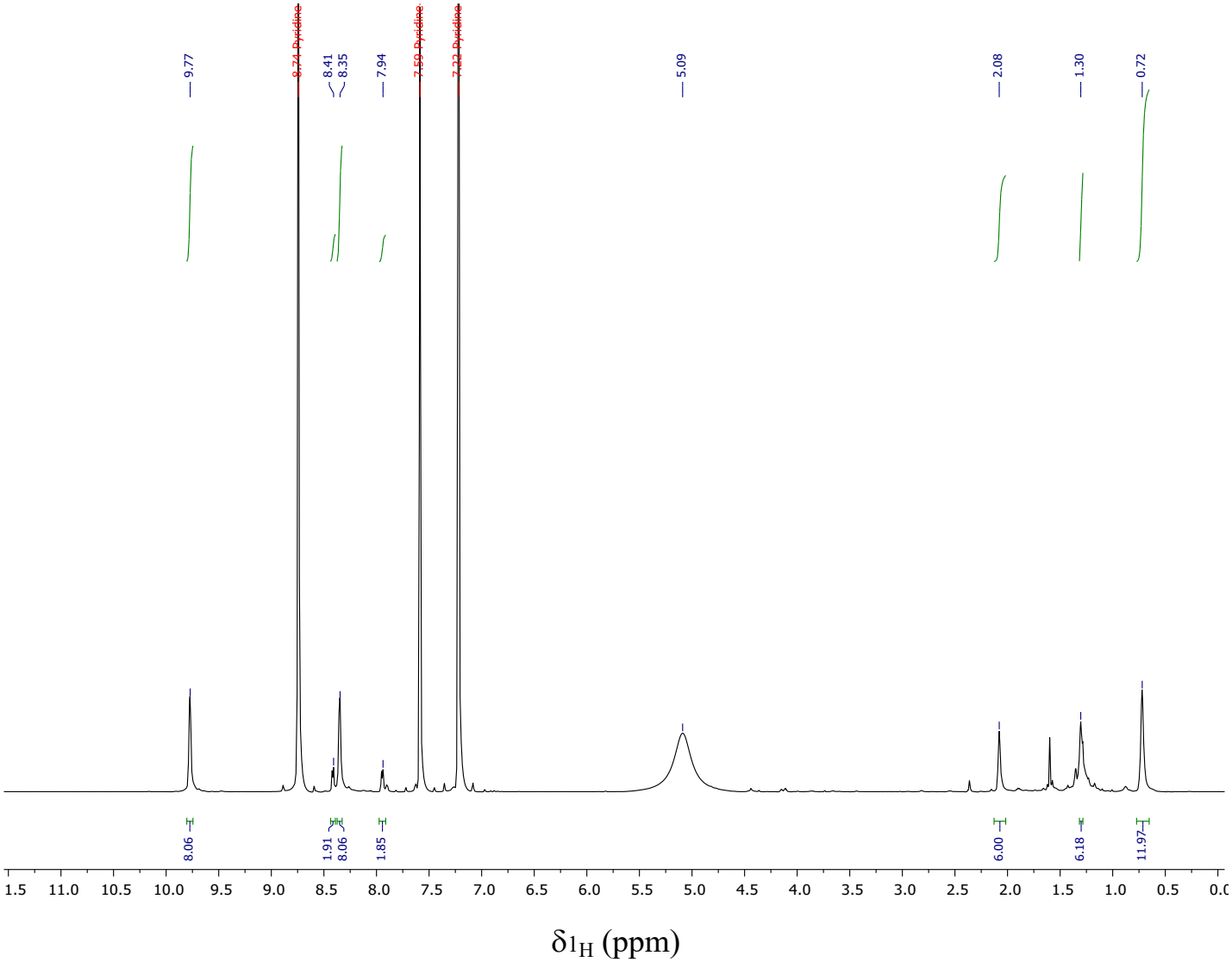

Figure S14. Solution ^{1}H NMR spectrum of the hybrid complex $FeNx_3$(B4-C_6H_4COOH)(ZrPc) in pyridine-d_5.

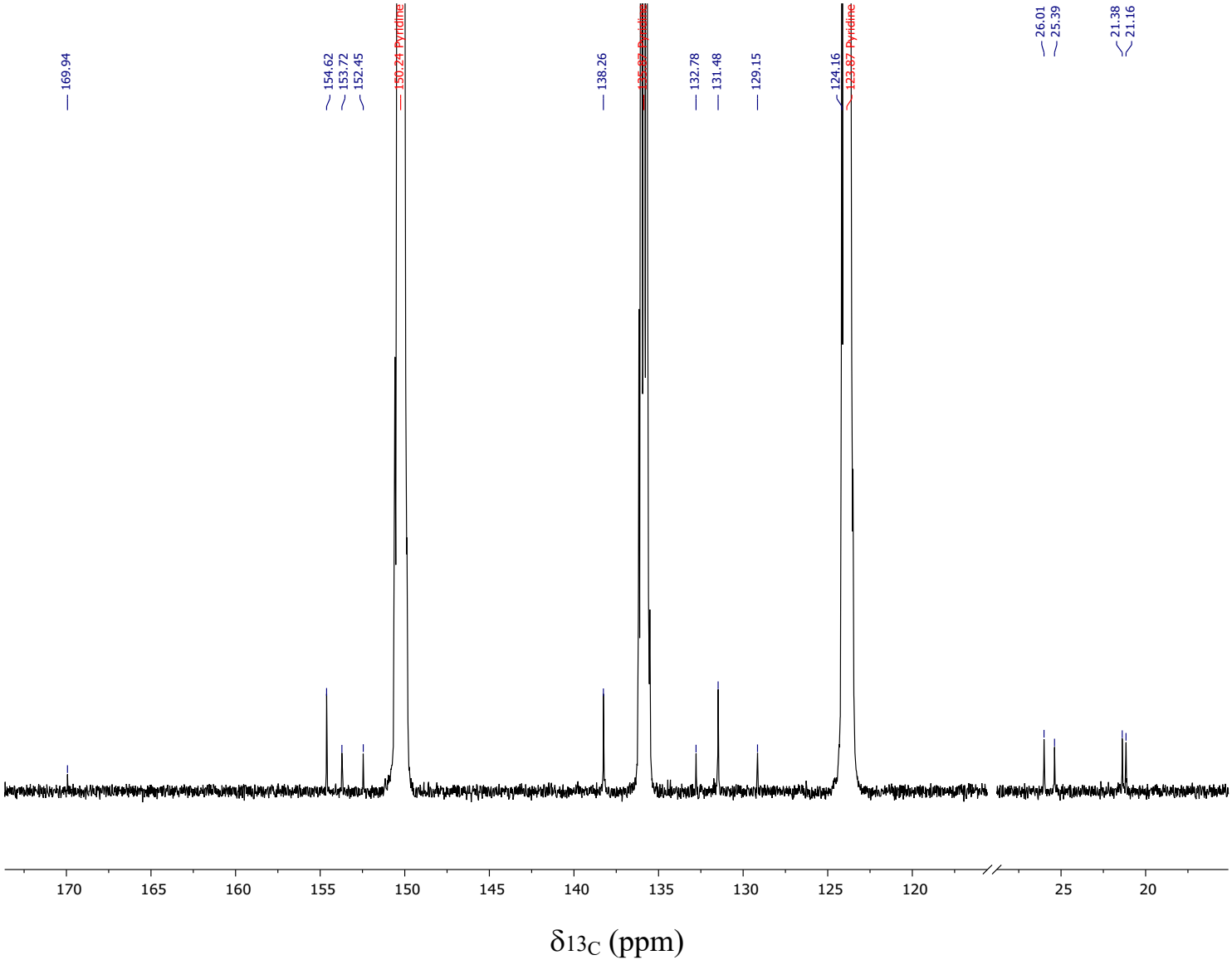

Figure S15. $^{13}C\{^{1}H\}$ NMR spectrum of the hybrid complex $FeNx_3(B4\text{-}C_6H_4COOH)(ZrPc)$ in pyridine-d_5.

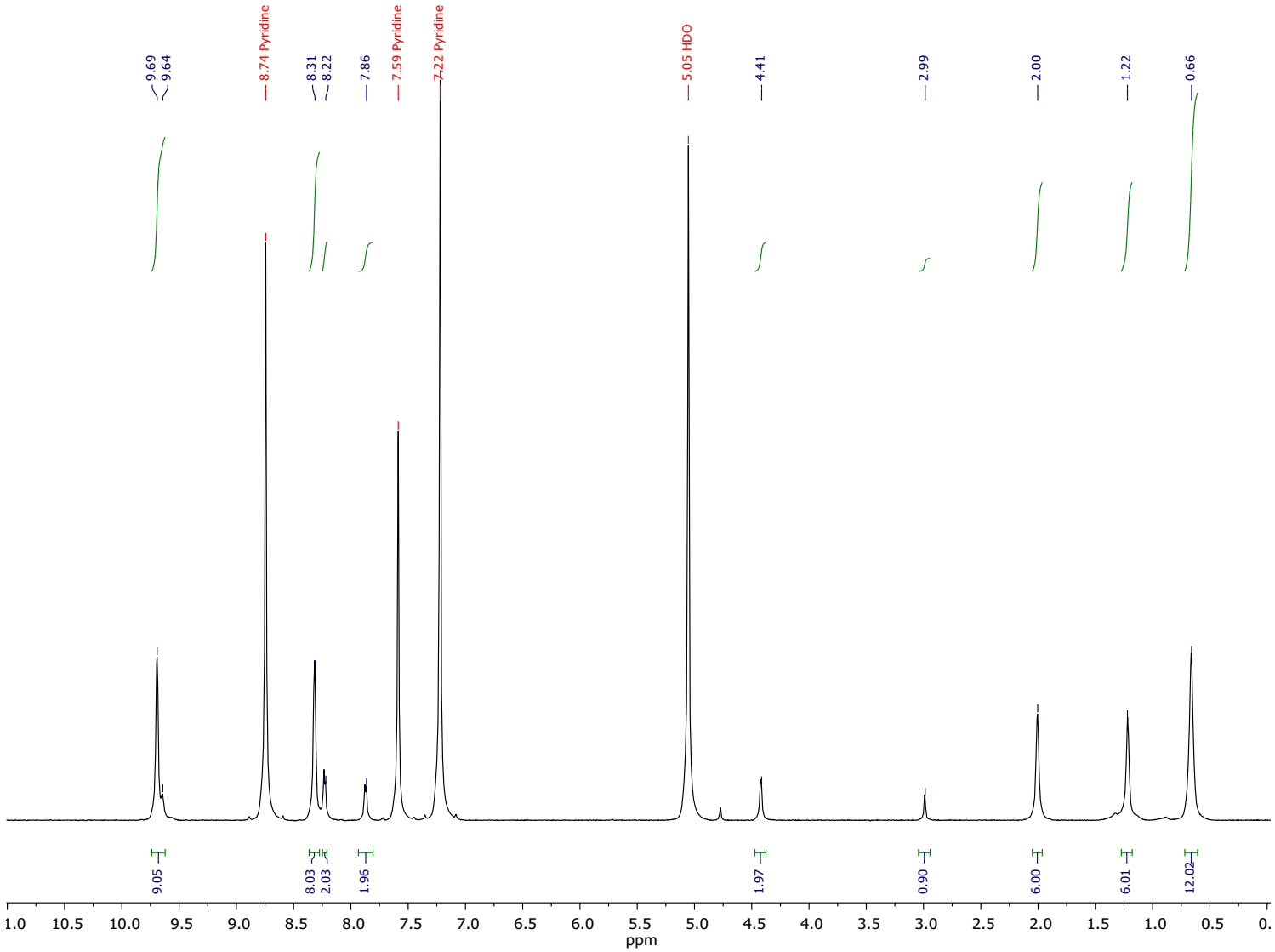

Figure S16. Solution ^{1}H NMR spectrum of the hybrid complex $FeNx_3$(B4-C_6H_4COProp)(ZrPc) in pyridine-d_5.

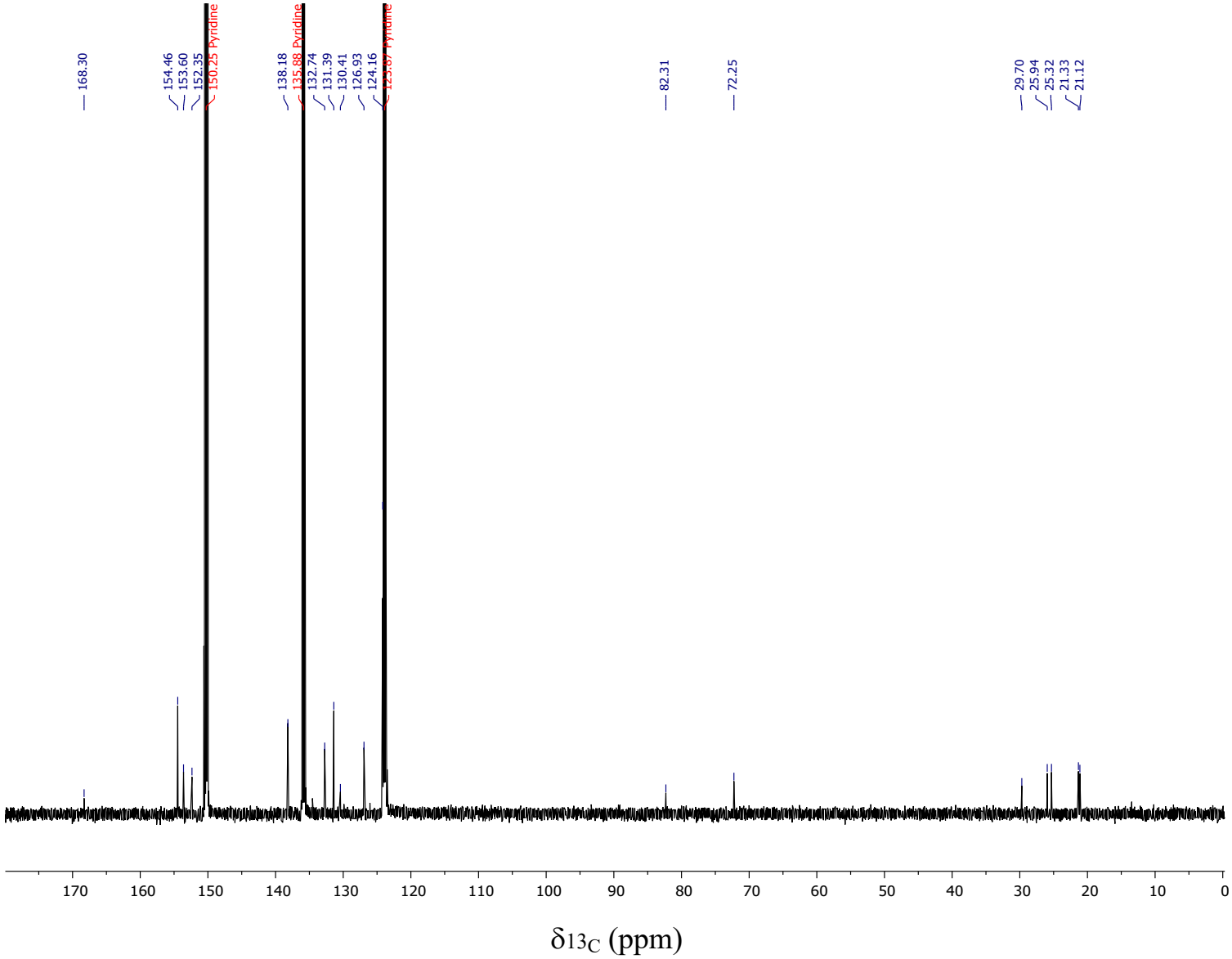

Figure S17. Solution $^{13}C\{^{1}H\}$ NMR spectrum of the hybrid complex $FeNx_3$(B4-C_6H_4COProp)(ZrPc) in pyridine-d_5.

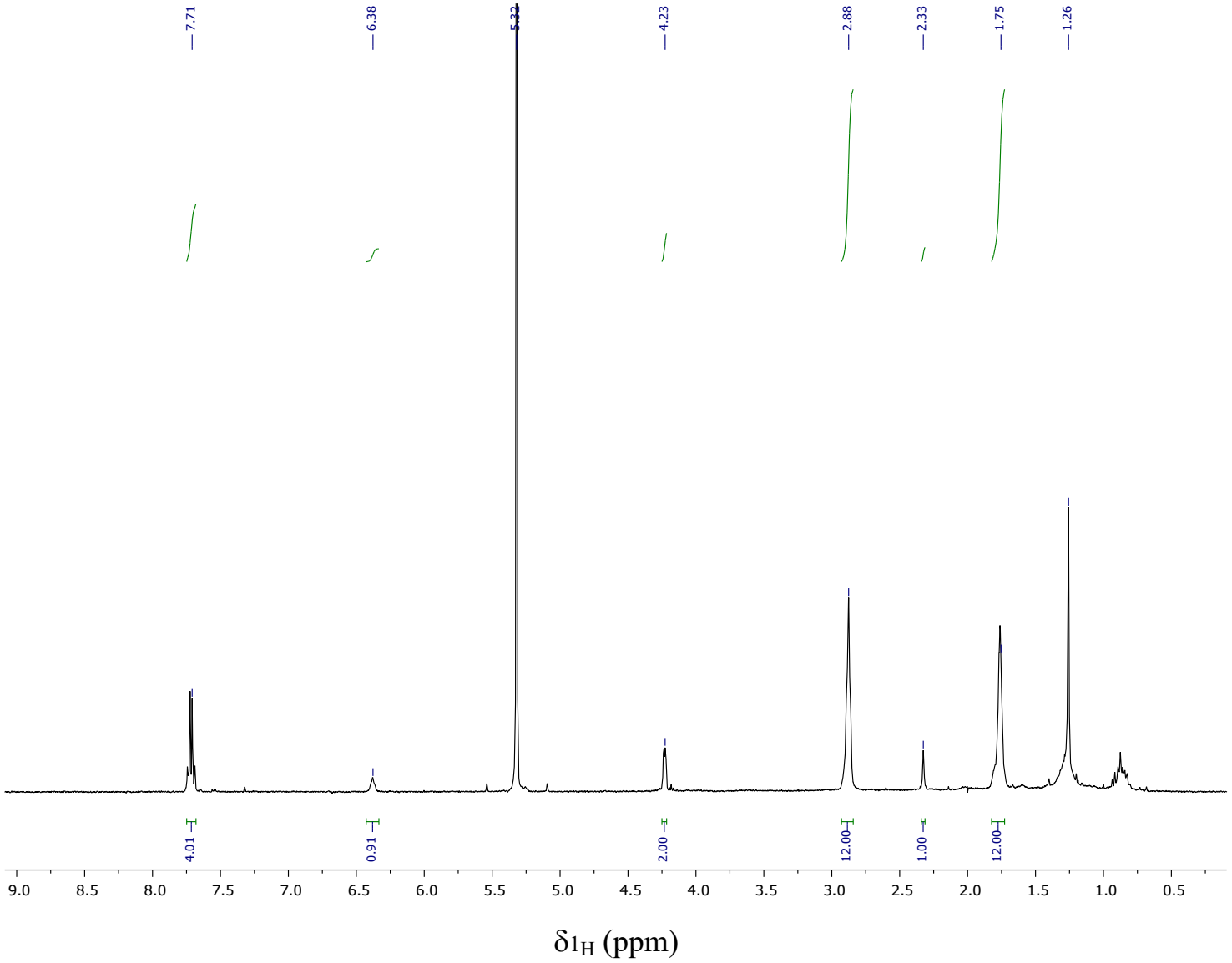

Figure S18. Solution ^{1}H NMR spectrum of the semiclatrochelate Fe(HNx)$_2$Nx(B4-C$_6$H$_4$COProp) in CD_2Cl_2.

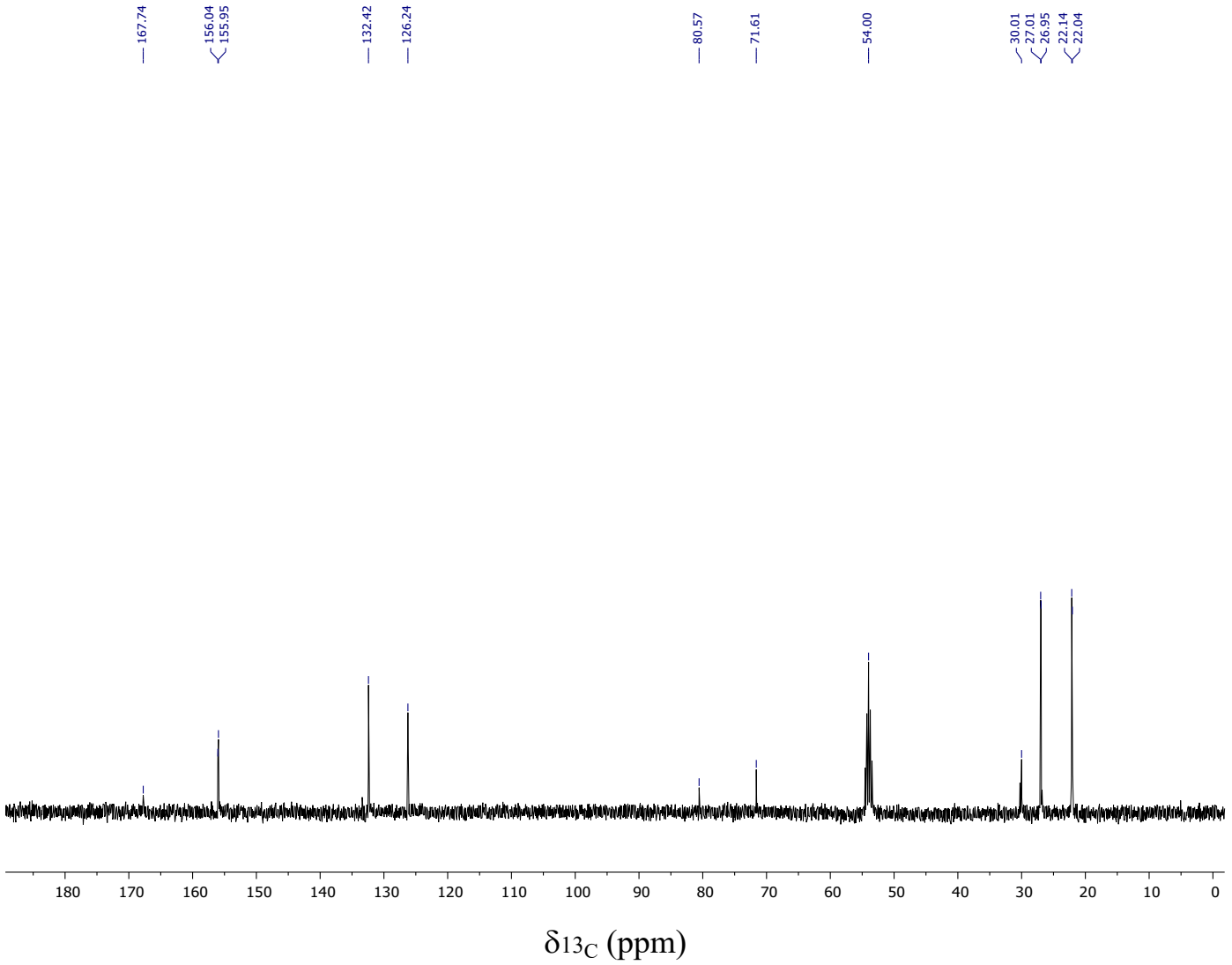

Figure S19. Solution ^{13}C ^{1}H NMR spectrum of the semiclatrochelate $Fe(HNx)_2Nx(B4\text{-}C_6H_4COProp)$ in CD_2Cl_2.

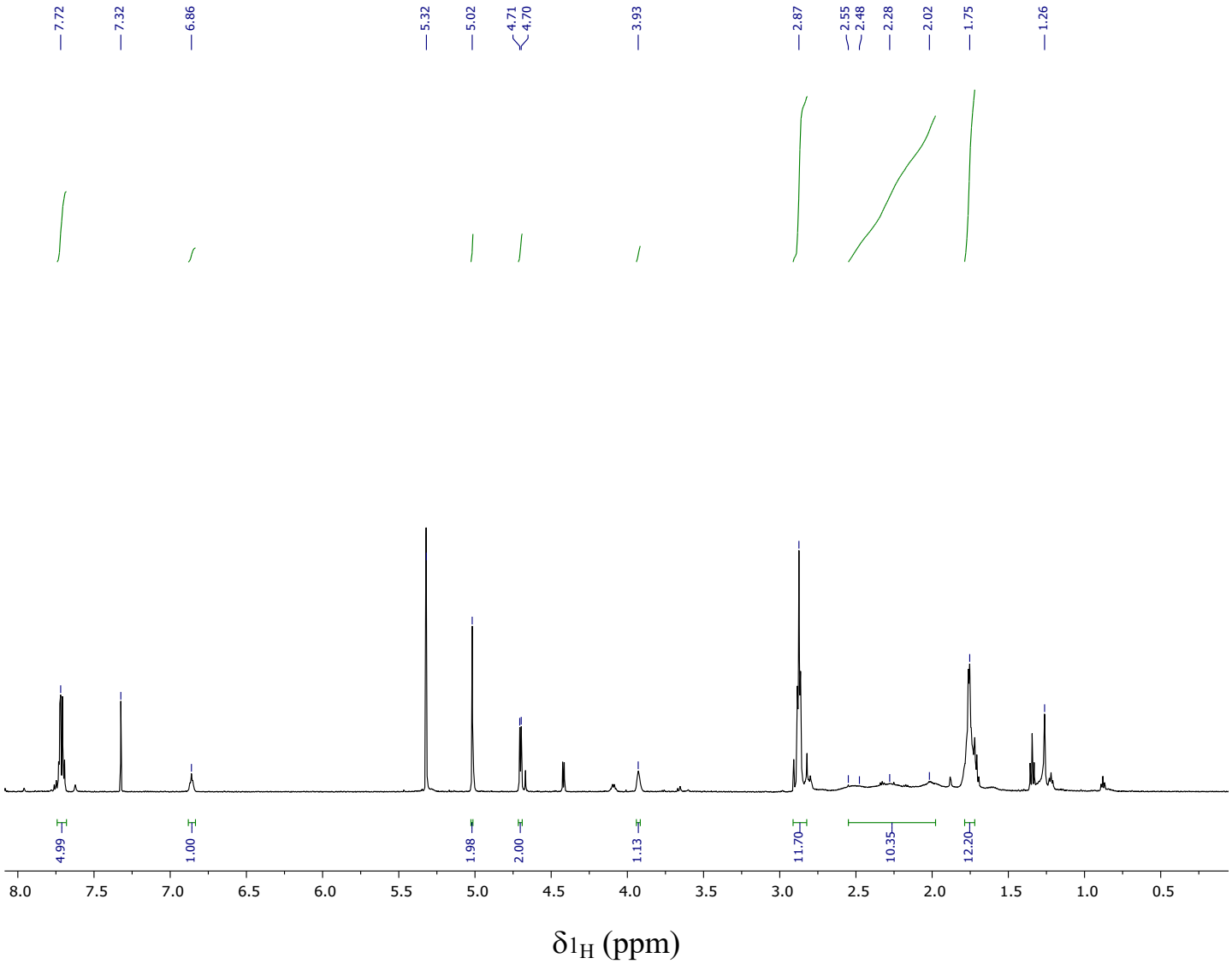

Figure S20. Solution ^{1}H NMR spectrum of the carboranosemiclatrochelate $Fe(HNx)_2Nx(B4\text{-}C_6H_4COSpCarb)$ in CD_2Cl_2.

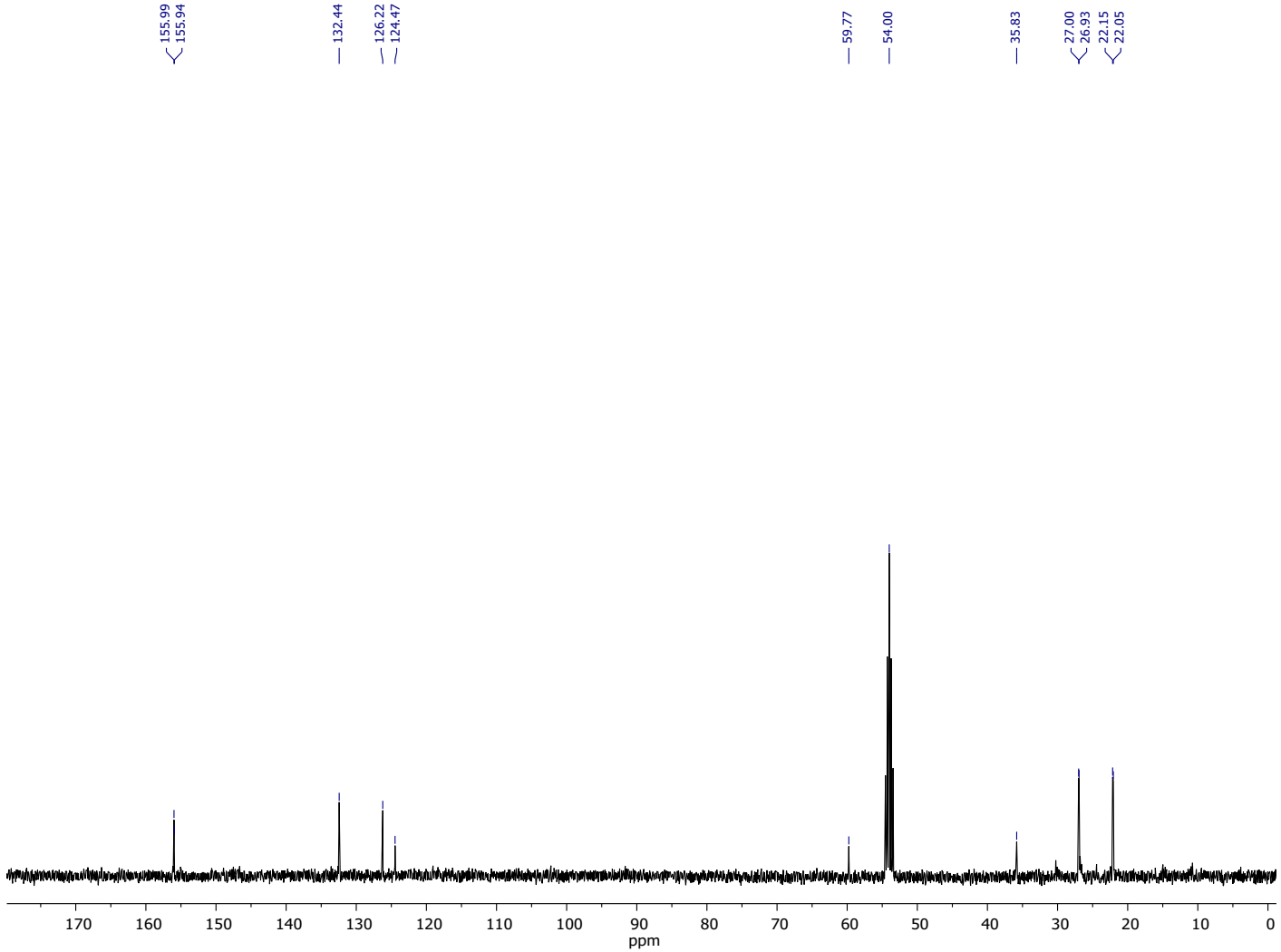

Figure S21. Solution $^{13}C\{^{1}H\}$ NMR spectrum of the carboranosemiclatrochelate $Fe(HNx)_2Nx(B4\text{-}C_6H_4COSpCarb)$ in CD_2Cl_2.

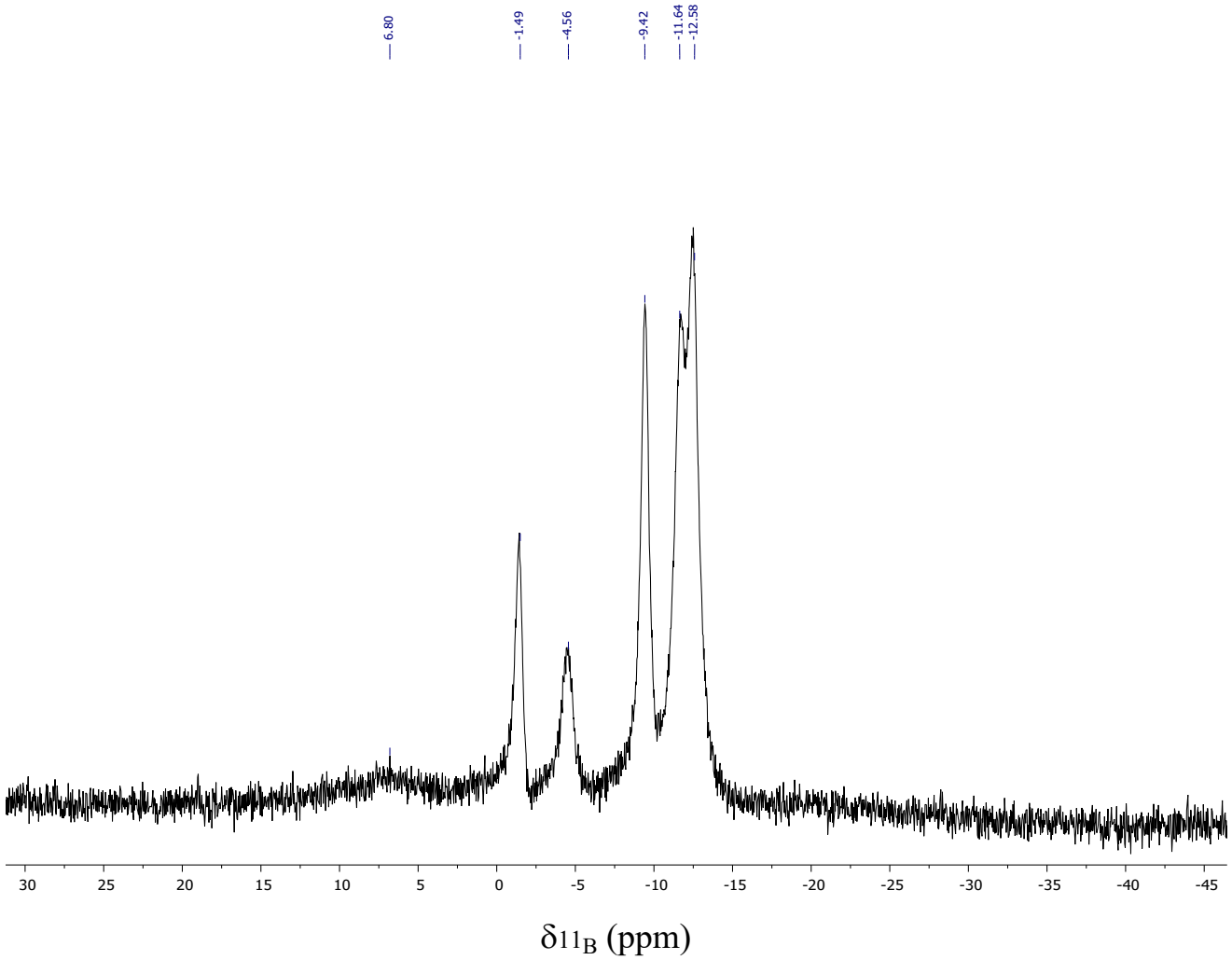

Figure S22. Fragment of the solution $^{11}B\{^{1}H\}$ NMR spectrum of the carboranosemiclatrochelate $Fe(HNx)_2Nx(B4\text{-}C_6H_4COSpCarb)$ in CD_2Cl_2.

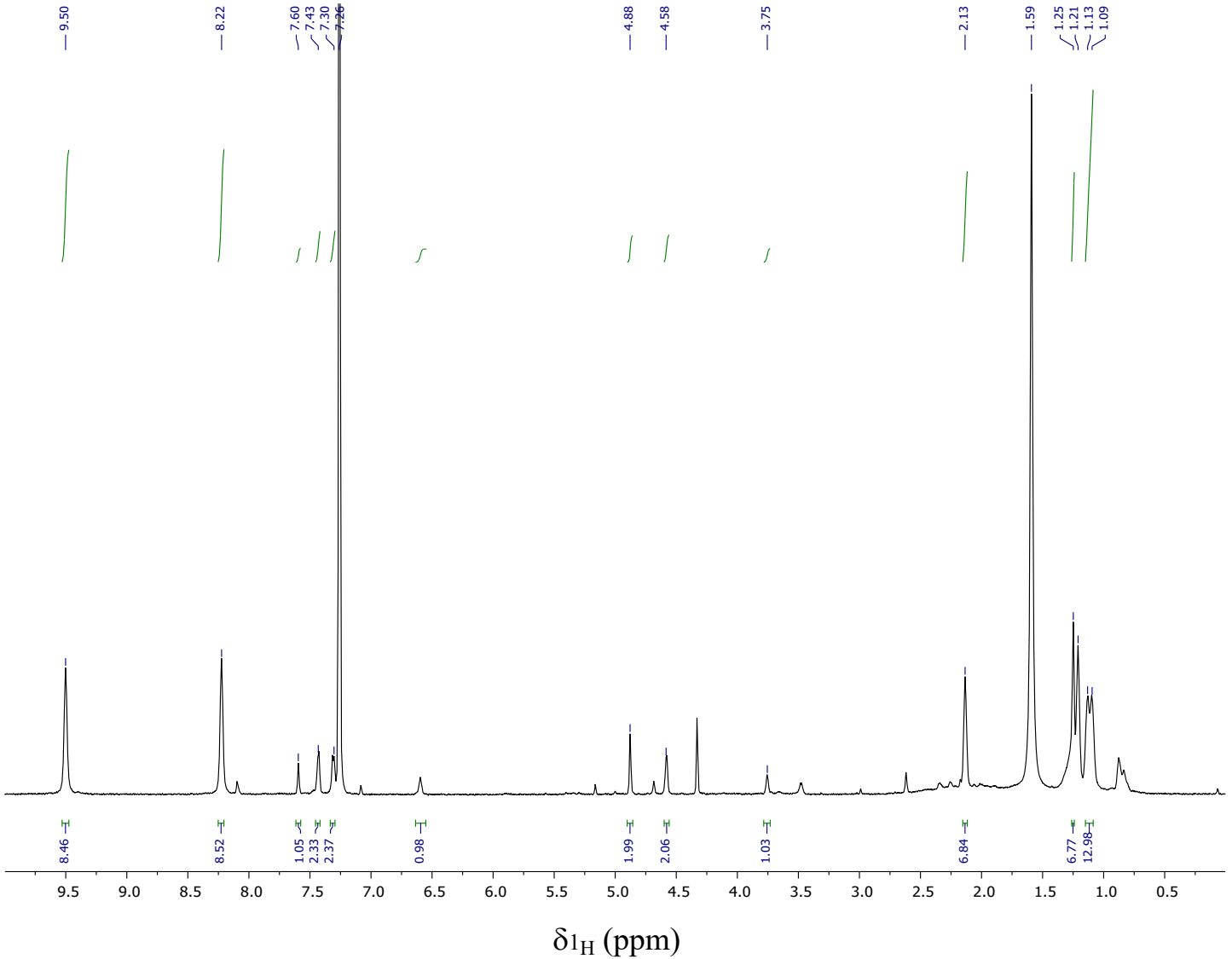

Figure S23. Solution ^{1}H NMR spectrum of the polytopic complex $FeNx_3$(B4-C_6H_4COSpCarb)(ZrPc) in $CDCl_3$.

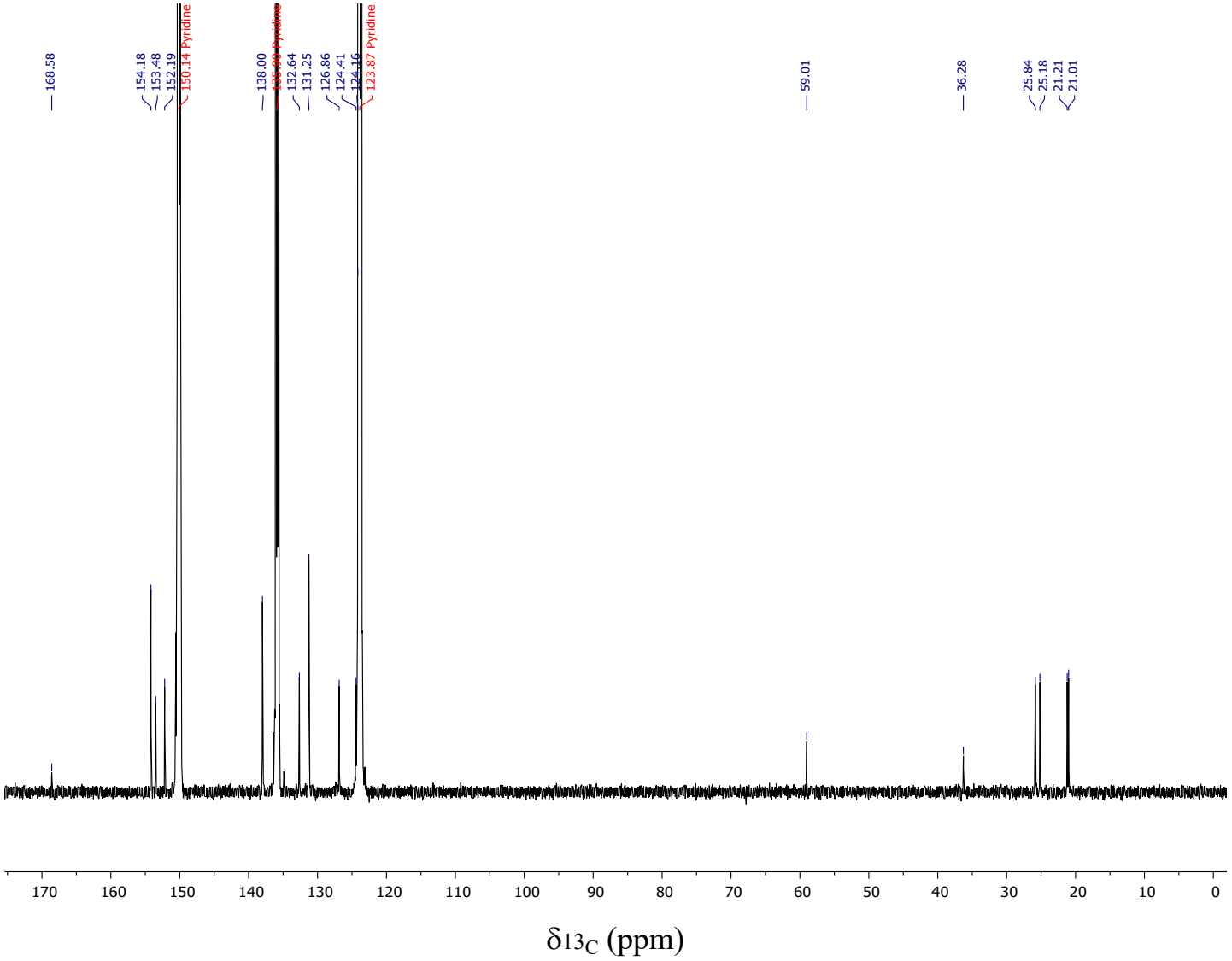

Figure S24. Solution $^{13}C\{^{1}H\}$ NMR spectrum of the polytopic complex $FeNx_3(B4\text{-}C_6H_4COSpCarb)(ZrPc)$ in pyridine-d_5.

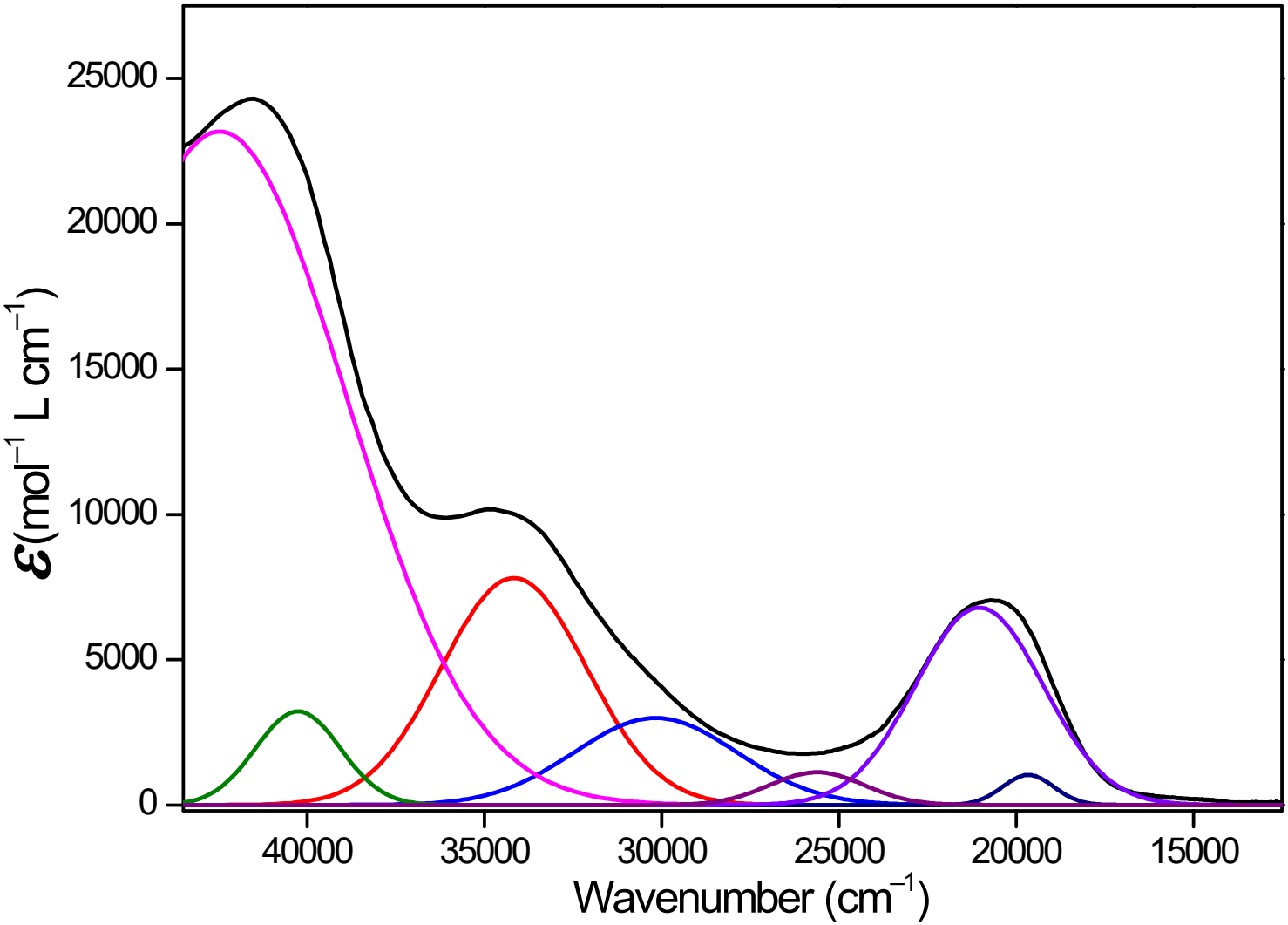

Figure S25. Solution UV-vis spectrum of the semiclathrochelate $FeNx(HNx)_2(B4\text{-}C_6H_4COOH)$ in CH_2Cl_2 (shown in black line) and its deconvolution into the Gaussian components (shown in color lines).

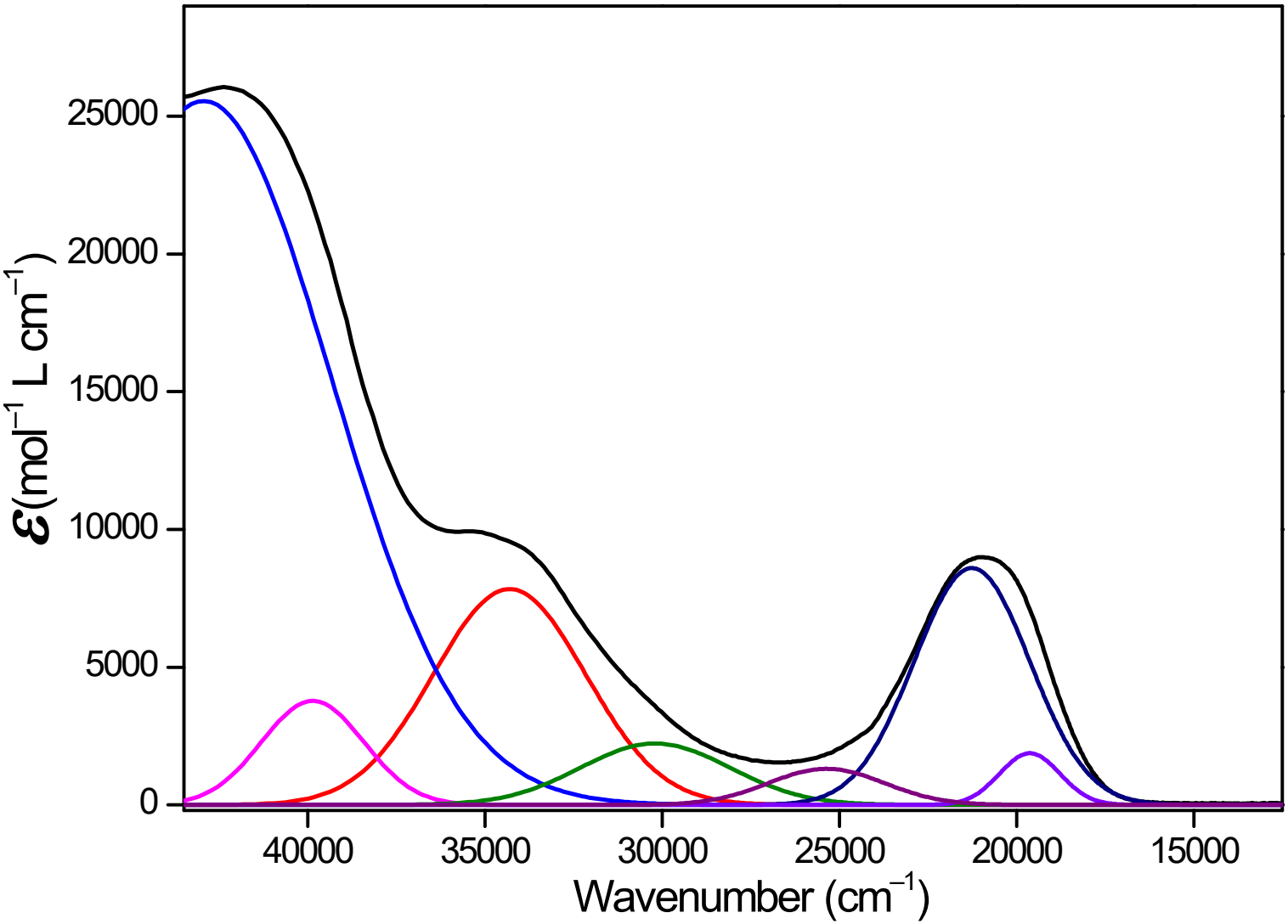

Figure S26. Solution UV-vis spectrum of the semiclathrochelate $FeNx(HNx)_2(B4\text{-}C_6H_4COProp)$ in CH_2Cl_2 (shown in black line) and its deconvolution into the Gaussian components (shown in color lines).

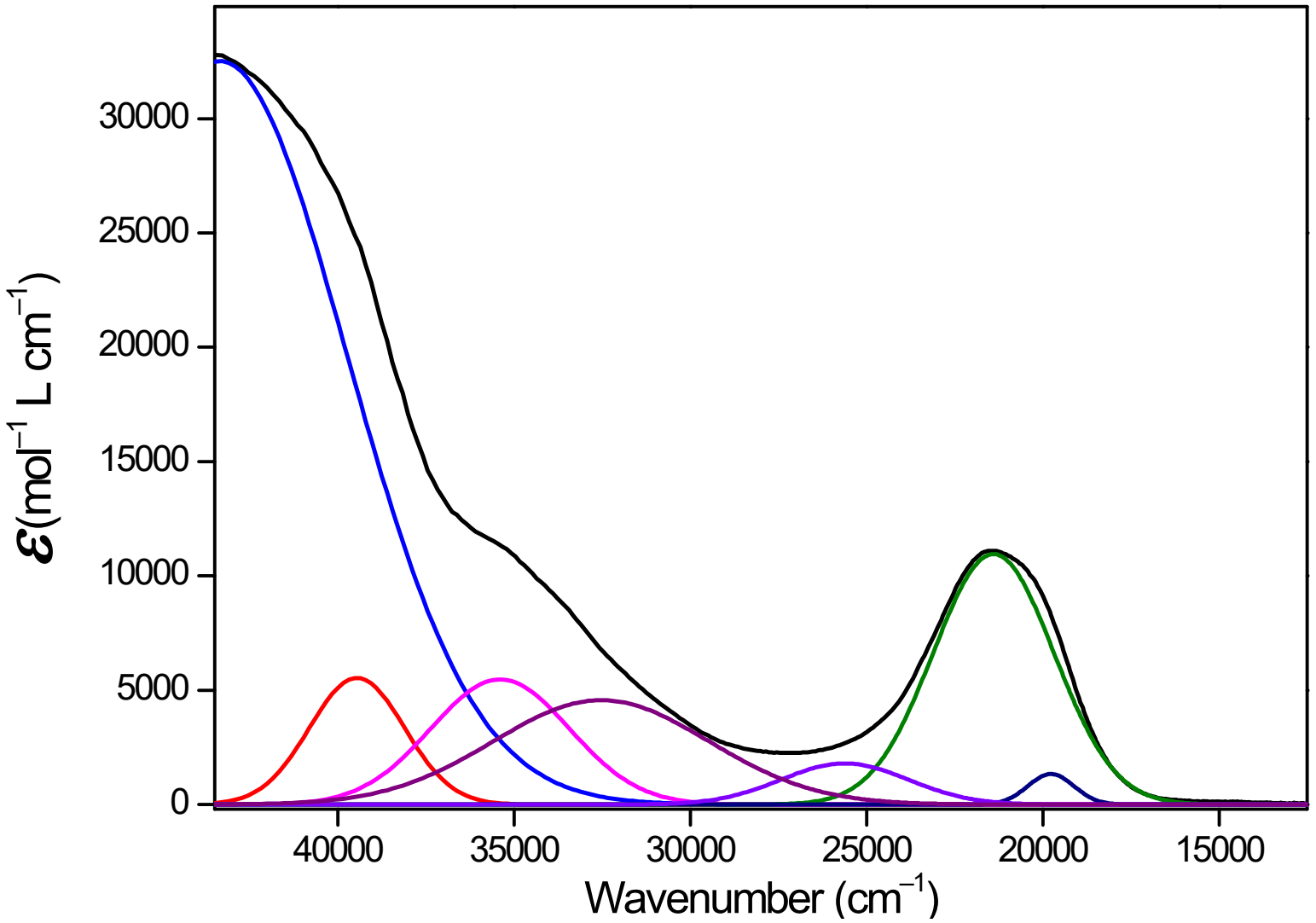

Figure S27. Solution UV-vis spectrum of the carboranosemiclathrochelate FeNx(HNx)$_2$(B4-C$_6$H$_4$COSpCarb) in CH_2Cl_2 (shown in black line) and its deconvolution into the Gaussian components (shown in color lines).

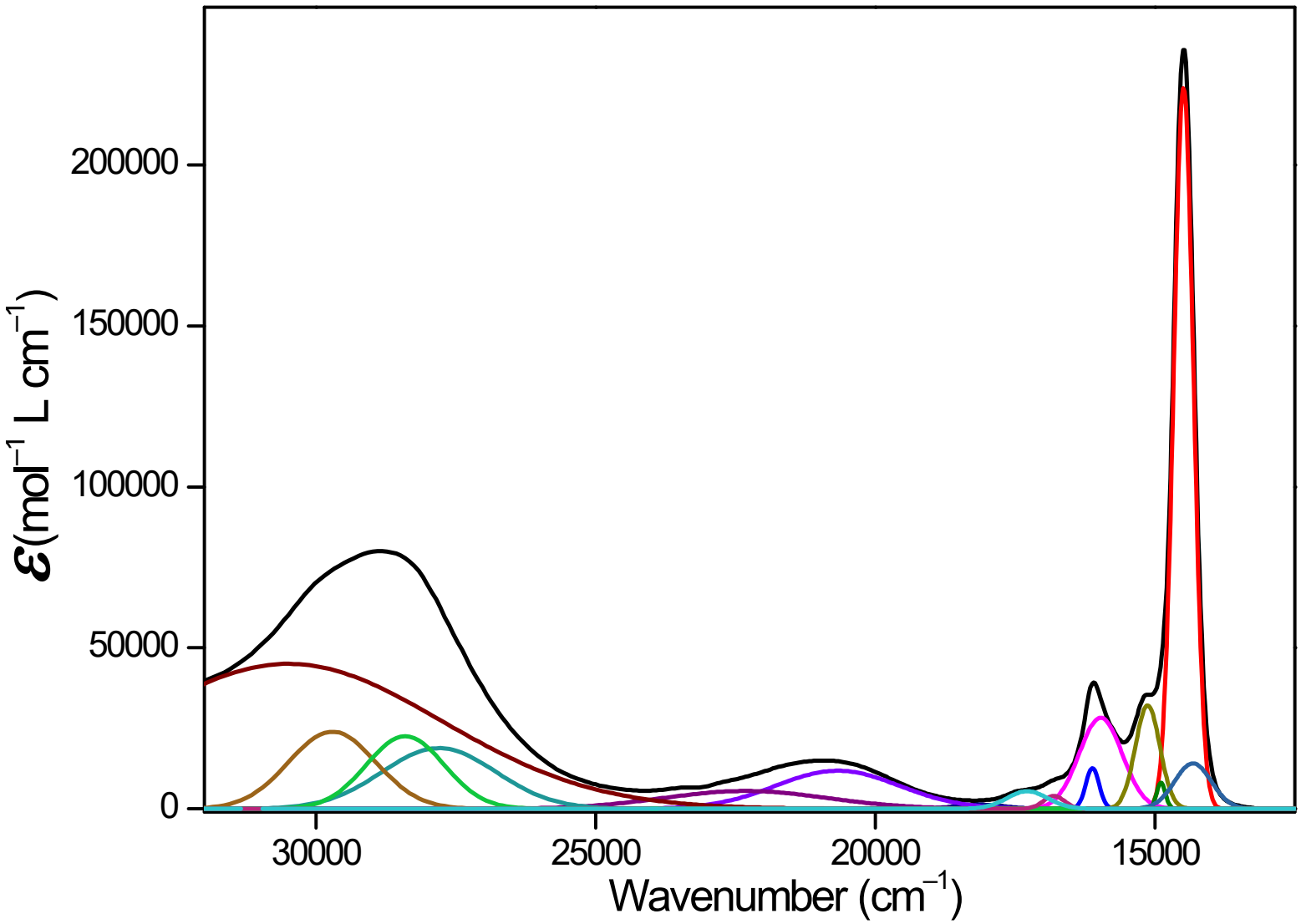

Figure S28. Solution UV-vis spectrum of the phthalocyaninatoclathrochelate $FeNx_3(B4\text{-}C_6H_4COOH)(ZrPc)$ in pyridine (shown in black line) and its deconvolution into the Gaussian components (shown in color lines).

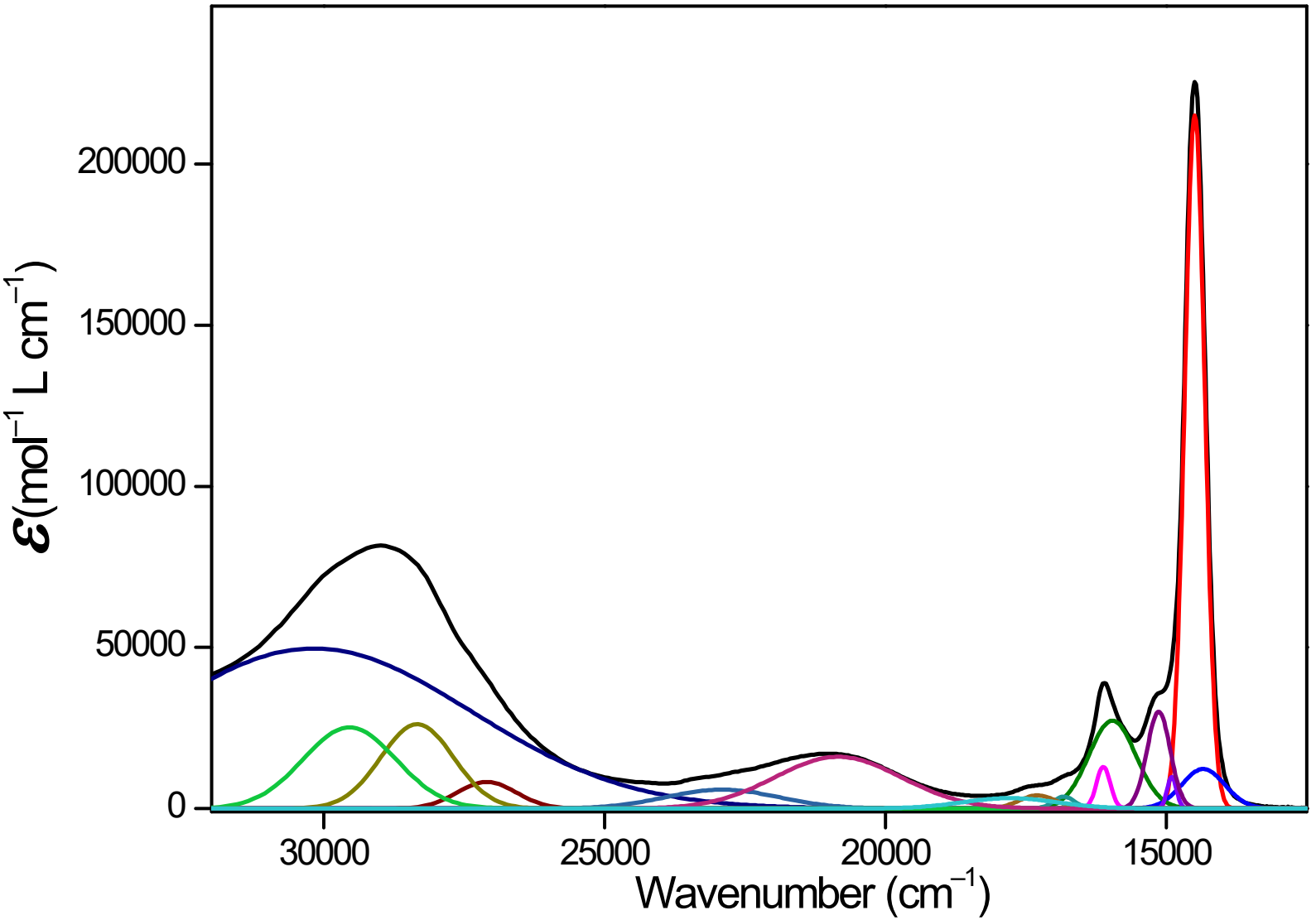

Figure S29. Solution UV-vis spectrum of the phthalocyaninatoclathrochelate $FeNx_3(B4\text{-}C_6H_4COOH)(HfPc)$ in pyridine (shown in black line) and its deconvolution into the Gaussian components (shown in color lines).

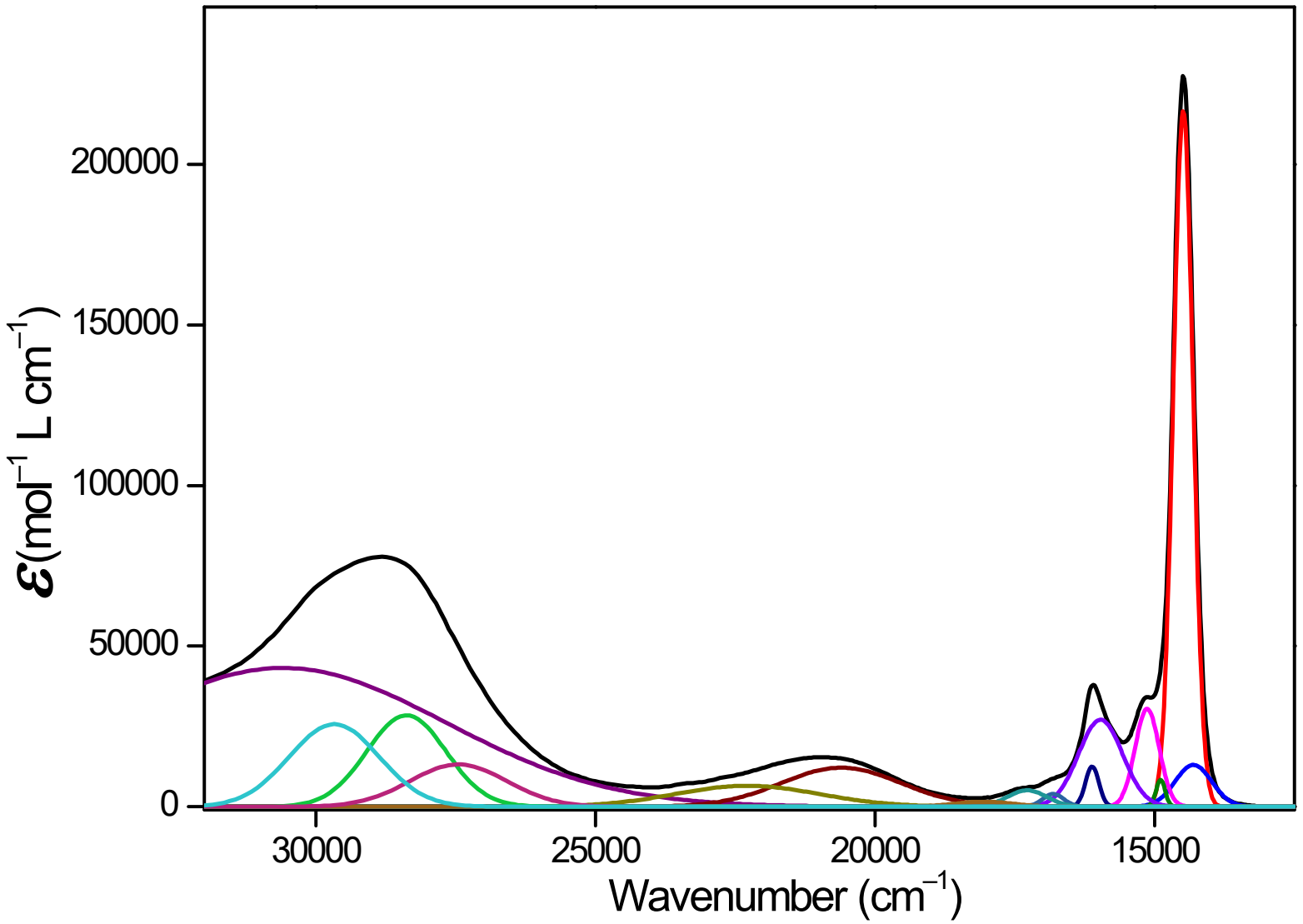

Figure S30. Solution UV-vis spectrum of the phthalocyaninatoclathrochelate $FeNx_3(B4\text{-}C_6H_4COProp)(ZrPc)$ in pyridine (shown in black line) and its deconvolution into the Gaussian components (shown in color lines).

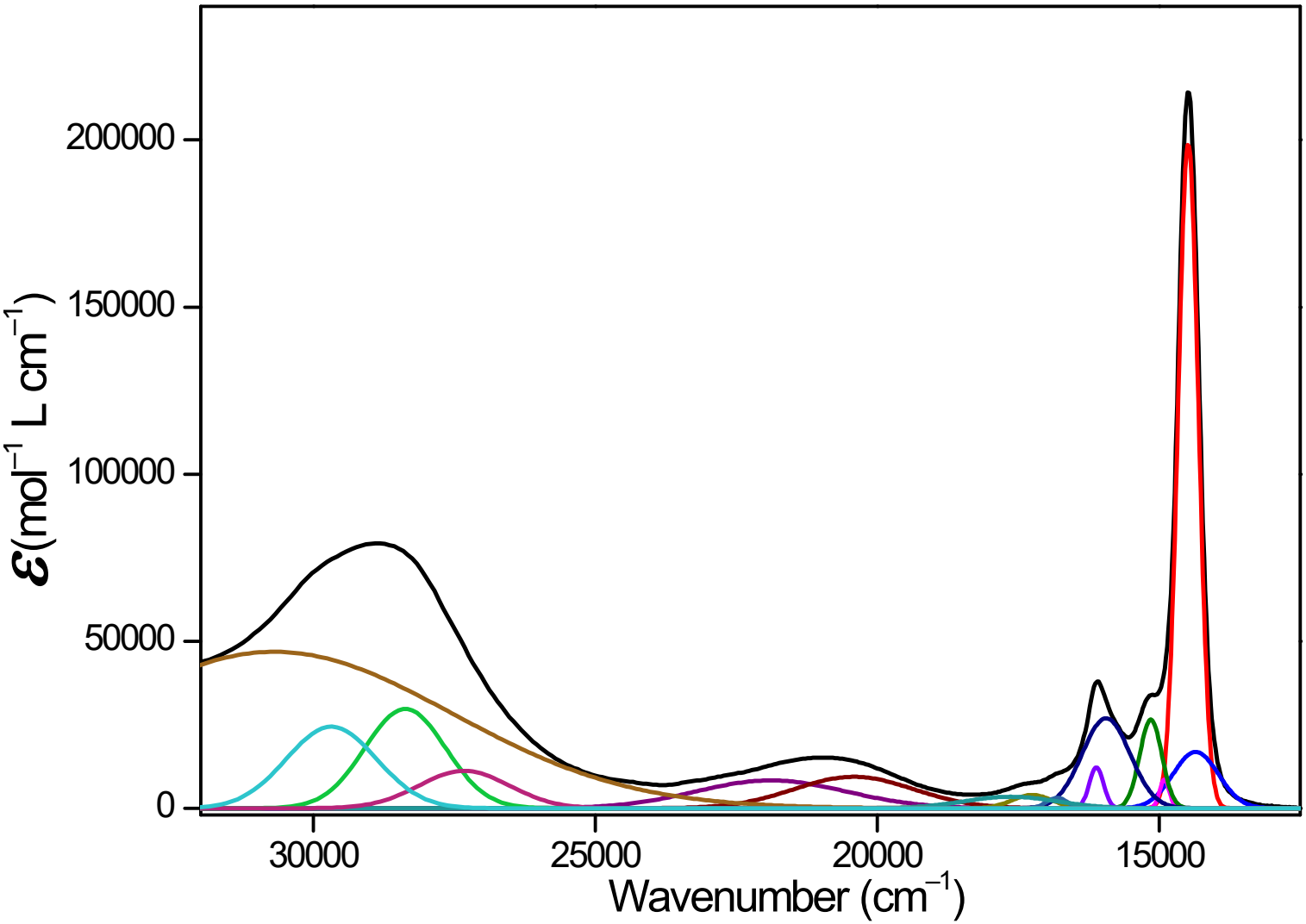

Figure S31. Solution UV-vis spectrum of the polytopic complex $FeNx_3$(B4-C_6H_4COSpCarb)(ZrPc) in pyridine (shown in black line) and its deconvolution into the Gaussian components (shown in color lines).

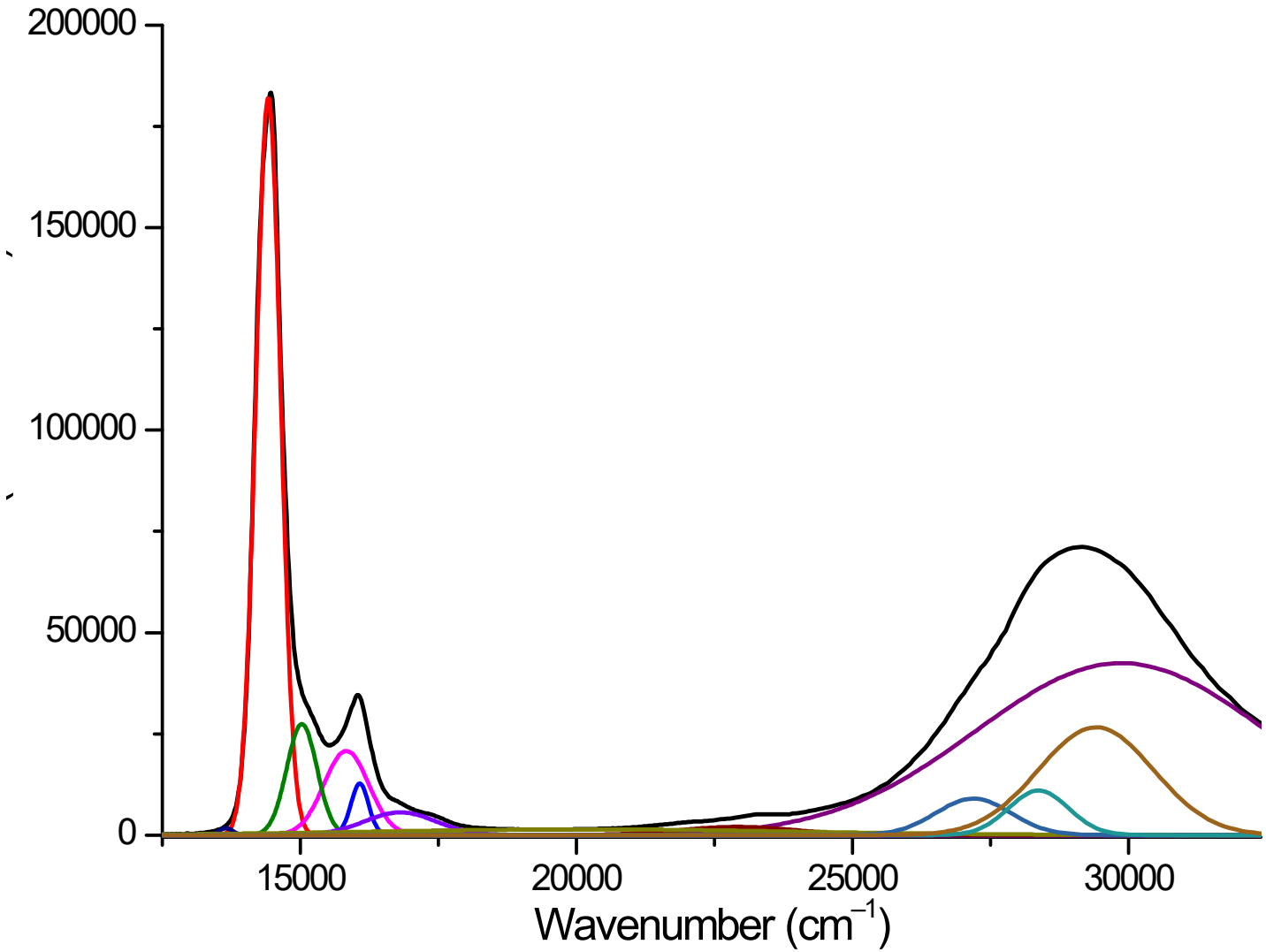

Figure S32. Solution UV-vis spectrum of the metallocomplex precursor $HfPcCl_2$ in pyridine (shown in black line) and its deconvolution into the Gaussian components (shown in color lines).

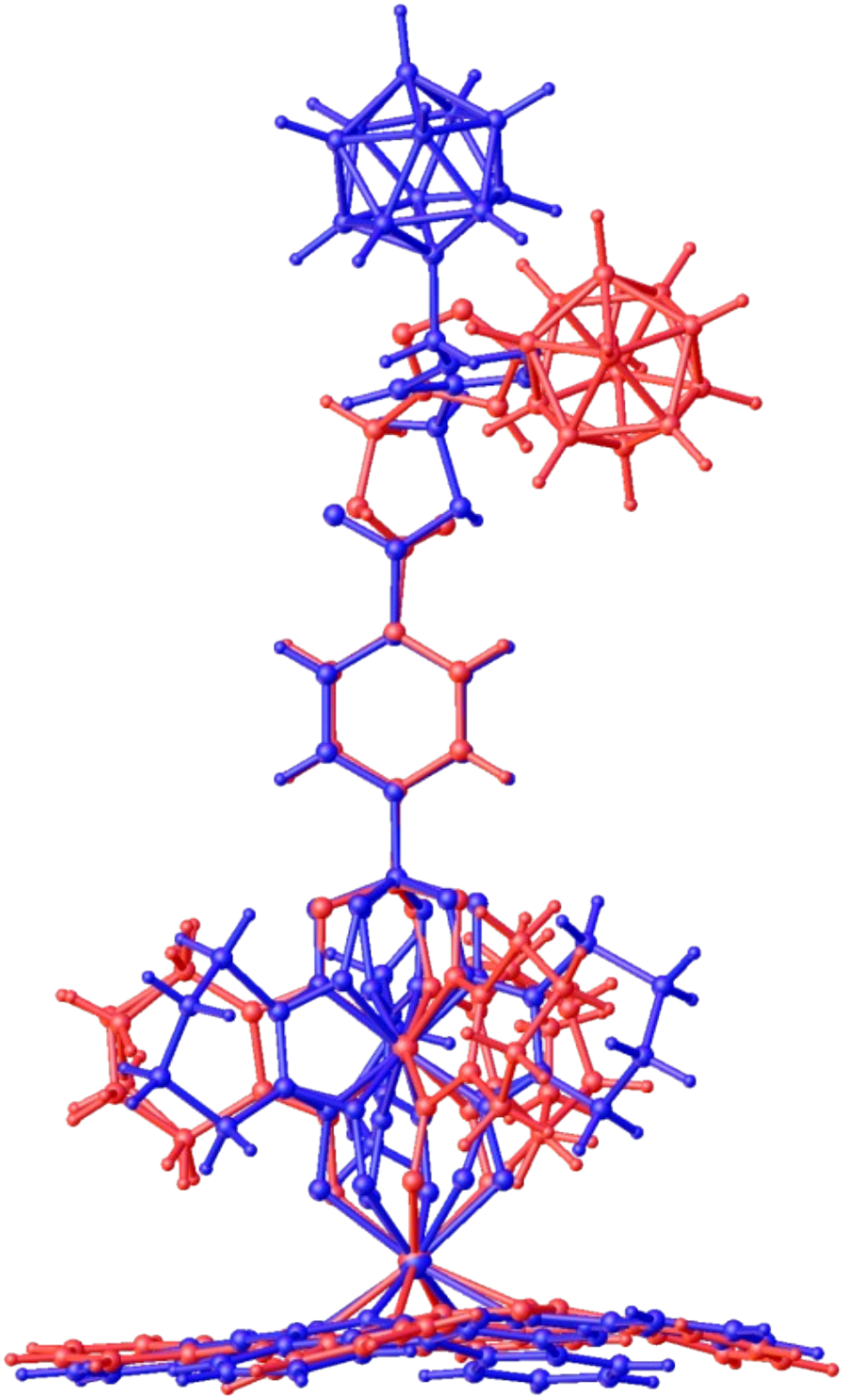

Figure S33. Comparison of the conformations of two symmetrically independent molecules of the polytopic carboranyl-terminated phthalocyaninatoclathrochelate $FeNx_3$(B4-C_6H_4COSpCarb)(ZrPc); their Zr, Fe and B atoms are overlaid.

Table S1. Solution UV-vis spectra (ν, cm^{-1}, $\varepsilon \times 10^{-3}$, $mol^{-1} \cdot L \cdot cm^{-1}$) of the obtained hybrid and polytopic iron(II) complexes

Compound	ν_1	ν_2	ν_3	ν_4	ν_5	ν_6	ν_7	ν_8	ν_9	ν_{10}	ν_{11}	ν_{12}	ν_{13}	ν_{14}	ν_{15}
$FeNx_3$(B4-C_6H_4COOH)(ZrPc)	30501	29714	28408	27802	22328	20677	18131	17284	16809	16120	15973	15132	14893	14489	14322
	(45)	(24)	(23)	(19)	(5.5)	(12)	(1.3)	(5.5)	(4.0)	(13)	(28)	(32)	(8.1)	(224)	(14)
$FeNx_3$(B4-C_6H_4COOH)(HfPc)	30180	29544	28338	27100	22909	20846	17788	17293	16824	16123	15961	15137	14904	14494	14343
	(50)	(25)	(26)	(8.3)	(5.9)	(16)	(3.2)	(4.1)	(3.7)	(13)	(27)	(30)	(9.9)	(215)	(12)
$FeNx_3$(B4-C_6H_4COProp)(ZrPc)	30598	29676	28384	27454	22289	20609	18057	17282	16814	16119	15969	15135	14895	14490	14307
	(43)	(26)	(28)	(13)	(6.5)	(12)	(1.6)	(5.1)	(3.9)	(12)	(27)	(31)	(8.4)	(217)	(13)
$FeNx_3$(B4-C_6H_4COSpCarb)(ZrPc)	30690	29682	28373	27326	21886	20419	17638	17255	16812	16115	15943	15150	14908	14485	14354
	(47)	(24)	(30)	(11)	(8)	(9.4)	(3.4)	(4.0)	(3.1)	(12)	(27)	(27)	(8.7)	(200)	(17)

Table S2. Solution UV-vis spectra (ν, cm^{-1}, $\varepsilon \times 10^{-3}$, $mol^{-1} \cdot L \cdot cm^{-1}$) of the obtained iron(II) semiclathrochelates and that of a model carborane-based compound.

Compound	ν_1	ν_2	ν_3	ν_4	ν_5	ν_6	ν_7
$FeNx(HNx)_2(B4\text{-}C_6H_4COOH)$	42475	40264	34171	30173	25620	21039	19661
	(23)	(3.2)	(7.8)	(3.0)	(1.1)	(6.8)	(1.0)
$FeNx(HNx)_2(B4\text{-}C_6H_4COProp)$	42949	39866	34311	30199	25365	21259	19628
	(26)	(3.8)	(7.8)	(2.2)	(1.3)	(8.6)	(1.9)
$FeNx(HNx)_2(B4\text{-}C_6H_4COSpCarb)$	43343	39462	35403	32533	25625	21399	19773
	(33)	(5.5)	(5.5)	(4.6)	(1.8)	(11)	(1.3)
1-[(*o*-carboran-1'-yl)methyl]-	45454	37879					
4-pentyl-1,2,3-triazole [S7]	(3.7)	(0.08)					

Table S3. Crystallographic data and structure refinement details for the semiclathrochelate, hybrid and polytopic iron(II) complexes under study

Compound	$Fe(HNx)_2Nx(B4\text{-}C_6H_4COOH)$	$Fe(HNx)_2Nx(B4\text{-}C_6H_4COProp)$	$FeNx_3(B4\text{-}C_6H_4COOH)(ZrPc) \cdot 2.5C_6H_6$	$(d_5\text{-Py}\cdot H)^+[FeNx_3(B4\text{-}C_6H_4COO^-)(HfPc)] \cdot 2d_5\text{-Py}$	$FeNx_3(B4\text{-}C_6H_4COProp)(ZrPc) \cdot 1.5CH_2Cl_2$	$FeNx_3(B4\text{-}C_6H_4COSpCarb)(ZrPc)$
Formula	$C_{26}H_{33}BCl_2FeN_6O_8$	$C_{28}H_{34}BFeN_7O_7$	$C_{72}H_{60}BFeN_{14}O_8Zr$	$C_{72}H_{44}BD_{16}FeHfN_{17}O_8$	$C_{61.5}H_{51}BCl_3FeN_{15}O_7Zr$	$C_{63}H_{61}B_{11}FeN_{18}O_7Zr$
Fw	695.14	647.28	1407.22	1552.61	1376.40	1448.27
Crystal system	Triclinic	Triclinic	Triclinic	Triclinic	Monoclinic	Triclinic
Space group	*P –1*	*P –1*	*P –1*	*P –1*	*P 2₁/n*	*P –1*
a (Å)	9.757(2)	9.970(2)	12.236(3)	14.080(3)	14.242(3)	19.422(4)
b (Å)	10.204(2)	11.030(2)	12.862(3)	16.520(3)	17.942(4)	20.591(4)
c (Å)	16.040(3)	13.310(3)	23.178(5)	17.020(3)	23.090(5)	21.089(4)
α (deg)	78.968(4)	87.32(3)	90.70(3)	73.19(3)	90	71.88(3)
β (deg)	77.178(4)	88.96(3)	93.99(3)	87.98(3)	93.33(3)	69.88(3)
γ (deg)	73.981(5)	78.04(3)	106.72(3)	64.78(3)	90	87.44(3)
Volume ($Å^3$)	1482.1(5)	1430.3(5)	3483.1(13)	3410.8(15)	5890(2)	7508(3)
Z	2	2	2	2	4	4
ρ_{calc} (g/cm^3)	1.558	1.503	1.342	1.512	1.552	1.281
μ (mm^{-1})	0.749	0.663	0.478	2.018	0.712	0.444
F(000)	720	676	1450	1556	2812	2968
Refls. collected	20425	32478	52706	33975	34977	27240
R_{int}	0.110	0.030	0.066	0.063	0.068	0.151
Data / restraints / parameters	9051 / 0 / 367	7487 / 0 / 396	19204 / 42 / 903	12067 / 36 / 897	12892 / 19 / 821	8746 / 1013 / 1419
Goodness-of-fit on F^2	0.999	1.06	1.06	1.04	1.06	1.63
R_1 [I>=2σ (I)]	0.082	0.042	0.060	0.050	0.074	0.109
wR2 [all data]	0.178	0.110	0.147	0.114	0.194	0.209
Largest diff. peak/hole (e $Å^{-3}$)	0.990 / –0.541	0.638 / –0.684	1.317 / –1.678	2.695 / –1.659	2.348 / –1.957	0.590 / –1.093

Supporting Information References

[S1] Y.Z.Voloshin, N.A.Kostromina, R.Krämer, *Clathrochelates: Synthesis, Structure and Properties*, Elsevier, 2002 and references therein.

[S2] Y.Z. Voloshin, E.V. Polshin, A.Y. Nazarenko, *Hyperfine Inter*. 2002, **141**, 309–320 and references therein.

[S3] Y.Z. Voloshin, O.A. Varzatskii, T.E. Kron, V.K. Belsky, V.E. Zavodnik, N.G Strizhakova, A.V. Palchik, *Inorg.Chem*., 2000, **39**, 1907–1918.

[S4] Y.Z. Voloshin, V.E. Zavodnik, O.A. Varzatskii, V.K. Belsky, A.V. Palchik, N.G. Strizhakova, I.I. Vorontsov, M.Y. Antipin, *Dalton Trans*. 2002, 1193–1202.

[S5] S.C. Bart, K. Chłopek, E. Bill, M.W. Bouwkamp, E. Lobkovsky, F. Neese, K. Wieghardt, P.J. Chirik, *J. Am. Chem. Soc*. 2006, **128**, 13921 – 13912.

[S6] S. Pillet, V. Legrand, H.-P. Weber, M. Souhassou, J.-F. Létard, P. Guionneau, C. Lecomte, *Z. Kristallogr*., 2008, **223**, 235–249.

[S7] G.E.Zelinskii, I.P.Limarev, A.V.Vologzhanina, V.A.Olshevskaya, A.V.Makarenkov, P.V.Dorovatovskii, A.S.Chuprin, M.A.Vershinin, S.V.Dudkin, Y.Z. Voloshin, *Molecules*. 2021, **26**, 3635.